Development of micro- and mesoporous ceramic-based materials for gas separation membranes

(ミクロおよびメソ多孔質セラミックス系ガス分離膜材料の開発研究)

2016

Mohd Nazri Mohd Sokri

Table of Contents

Chapter 1. Introduction

1.1. Membranes and separation technology

At the moment, about seventy percent of the world's primary energy sources comes from hydrocarbon fuels such as coal, petroleum and natural gas. However, most of these fuels are burnt in crude, dirty, and wasteful flame processes in engines and burners. It is predicted that combustion processes for energy production may be banned by the end of this century. Due to fossil fuel depletion and air pollution arising from its combustion, there is an urgent demand for renewable, clean fuel alternatives for future energy supply, of which hydrogen is rapidly becoming one of the leading candidates in meeting the world's energy needs. Hydrogen, a regenerative and environmentally friendly fuel with high calorific value, has attracted much attention by researchers. Hydrogen can be used in combustion devices and fuel cells without the production of polluting greenhouse gases. It can also be economical and have a relatively high margin of safety when properly produced, stored and dispensed.

Today, most hydrogen is produced through steam reforming of natural gas, described by the reaction:

$$CH_4 + H_2O \text{ (g)} = CO + 3H_2 \qquad \Delta H^o_{25°C} = 206 \text{ kJ/mol} \qquad (1\text{-}1)$$

$$CO + H_2O = CO_2 + H_2 \qquad \Delta H^o_{25°C} = -41 \text{kJ/mol} \qquad (1\text{-}2)$$
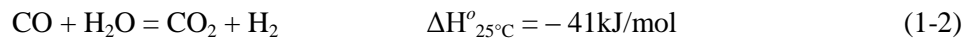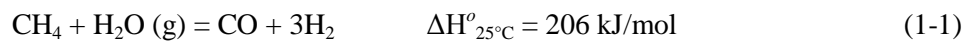
Eq. 1-1 is referred as the steam reforming reaction. This reaction is endothermic, and the conversion efficiency of methane (CH_4) / hydrogen (H_2) is restricted by thermodynamic equilibrium. It is usually performed in reformer tubes where the burning of the fuel gas provides the heat to drive the endothermic and thermodynamically controlled reforming reaction [1]. Generally, the reactor is operated at approximately 800°C. The resulting syngas then proceeds to a water-gas shift reactor to produce additional H_2 and carbon dioxide (CO_2) as shown in Eq. 1-2. Finally, the purified H_2 can be obtained using pressure swing adsorption (PSA) which adsorbed impurities from the syngas stream. Although commercially used for H_2 production, this steam reforming process is not particularly efficient mainly due to high operating temperature and several complicated purification steps [2] which leads to high cost of H_2 production that limits supplying H_2 as an alternative to the conventional hydrocarbon fuels. Thus, the development of more sustainable processes for energy conservation is globally demanded, in which membrane separation has received considerable attention as one of the key technologies for efficient energy production. Furthermore, increasing attention has been directed to the application of membranes for gas separation, especially for the production of high-purity hydrogen [3]. Gas separation is an essential process in energy generation processes such as

steam reforming as described above, coal gasification, biogas production [4] and dehydration in the energy recycle system by use of chemical organic hydrides [5] in order to extract energy carriers such as H_2 or CH_4 from mixed gas streams, to capture CO_2 from combustion processes [6], or to remove H_2O or H_2S from hydrocarbon streams [7].

In addition to application for the high-temperature hydrogen production process using steam reforming of methane, novel solar hydrogen production system (Fig. 1-1) has been found to be another attractive application [8]. Photocatalytic water splitting is an artificial photosynthesis process with photocatalysis in a photoelectrochemical cell used for the separation of water (H_2O) into hydrogen (H_2) and oxygen (O_2) with the presence of natural or artificial light. Theoretically, only solar energy (photons), water, and a catalyst are needed. This system has been considered as an environmentally friendly, hydrogen production can be acquired at relatively low temperature, and low cost since it utilizes water, an inexpensive renewable resource.
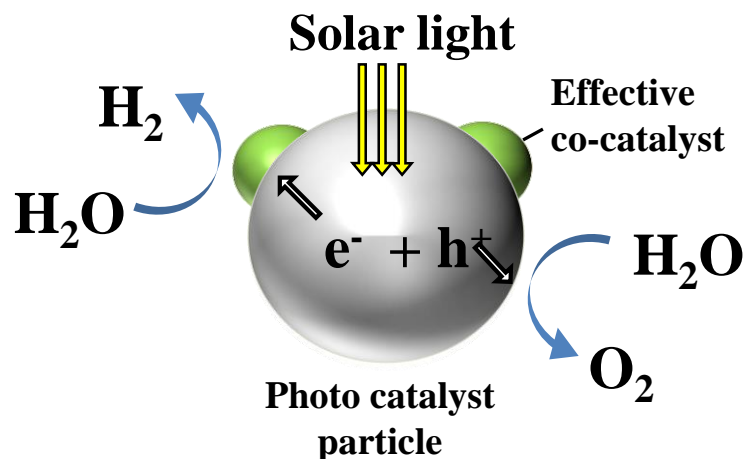
Fig. 1-1. Photocatalytic water splitting process from solar light for H_2 production.

However, in this system, it is required to separate H_2 from O_2 under the co-existence of H_2O at temperature below 100°C since H_2 and O_2 explosively react in the wide ratio of $H_2/O_2 =$ 0.0416-15.7 [9]. Thus, the novel development of materials having hydrophobicity characteristic is essentially demanded where H_2O can be effectively removed from the system, which leads to the high-purity hydrogen production.

Typically, there are two types of inorganic membranes considered for hydrogen separation: dense palladium- based membranes and porous ceramic membranes. Palladium-based membranes have been known to exhibit an excellent H_2 permselectivity. However, they are very expensive, susceptible to poisoning by sulphur and formation of pinholes or cracks as a result of

hydrogen embrittlement. Organometallic precursors-derived ceramic membranes with pore size smaller than one nanometer possess great potential for gas separation. In comparison to polymer membranes, microporous ceramic membranes have relatively high gas permeances and thermally stable, which have been expected to be used in hydrogen separation membranes. Amorphous silica-based membranes with molecular sieve-like properties have been widely studied for microporous ceramic membranes. Owing to their intrinsic microporosity, microporous silica-based membranes can effectively separate H_2 from other larger gas molecules such as CO_2 and N_2. However, microporous amorphous silica-based membranes exhibited low performance at temperature below 300°C [10]. In addition, amorphous silica-based membrane is essentially hydrophilic and the presence of H_2O in the membrane system would degrade the H_2 permselectivity due to adsorption followed by condensation of H_2O on their surface. Hence, this few drawbacks should be effectively addressed so that the novel development of H_2-pemselective separation membrane could be achieved.

1.2. Gas transportation mechanism related to the pore size

Gas separation mechanisms differ for porous membranes and dense (non-porous) ones. Depending on the pore sizes in membrane matrix, transport and separation mechanisms in porous membranes can be classified into viscous or Poiseuille flow, Knudsen diffusion, surface diffusion, capillary condensation and molecular sieving. Meanwhile, in dense membranes, the transport mechanism is typically governed by solution diffusion. The mechanisms mentioned are illustrated as shown in Fig. 1-2.

(a)   (b)   (c)   (d)   (e)   (f)
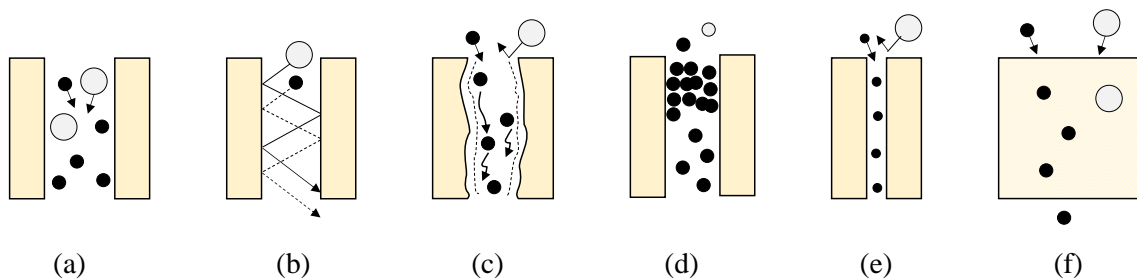
Fig 1-2. Gas separation mechanisms in porous/non-porous membranes of: (a) viscous flow, (b) Knudsen diffusion, (c) surface diffusion, (d) capillary condensation, (e) molecular sieving and (f) solution diffusion.

1.2.1. Viscous flow (Poiseuille flow)

The viscous, or Poiseuille flow mechanism occurs when the average pore diameter is bigger than the mean free path of the gas molecules and transport is occur by bulk fluid flow through the large pores. The mean free path here refers to the average distance travelled by a gas

molecule between collisions and it is pressure and temperature dependent. In this condition, membrane contains pores large enough to allow convective flow, where gas molecules collide exclusively with each other and no selective separation takes places between the gas components [11].

The Fick's law is commonly applied in basic problems to estimate permeation through a membrane and can be modified to give the following final expression:

$$J = -\frac{P\,(p_2 - p_1)}{\delta} \tag{1-3}$$

where J ($mol.m^{-2}.s^{-1}$) is the diffusion flux, P ($mol.m^{-1}.s^{-1}.Pa^{-1}$) is the permeability of the membrane, p_1 (Pa) is the pressure of the feed side, p_2 (Pa) is the pressure of the permeate side and δ (m) is the thickness of the membrane.

By assuming that the fluid is Newtonian, the following expression for the average velocity v ($m.s^{-1}$), may be derived, where d_p (m) is the diameter of the pore, μ (Pa.s) is the viscosity, l (m) is the length of the pore, p_o (Pa) is the inlet pressure, and p_L (Pa) is the pressure at a distance L (m).

$$v = \frac{d_p{}^2}{32\mu l}(p_o - p_L) \tag{1-4}$$

With appropriate manipulation, the following flux can be obtained:

$$J = \frac{Q_M}{L}(p_o - p_L) \tag{1-5}$$

By considering the porosity ε (-) and tortuosity τ (-) of the membrane, and the pore area per total volume, a (m^{-1}), which is related to the pore area per membrane volume a_v (m^{-1}), the following gas permeances expressions can be obtained:

$$Q_M = \frac{\rho\varepsilon^3}{2(1-\varepsilon)^2\mu\tau a_v{}^2} \quad \text{where} \quad a_v = \frac{a}{(1-\varepsilon)} \tag{1-6}$$

This type of transport mechanism is generally observed for the membranes having the much larger pore sizes than gas molecules, such as flow of a gas molecules permeating through a macroporous support with pore diameter, dp > 50 nm.

1.2.2. Knudsen diffusion

Knudsen diffusion occurs when the pore diameter is smaller than the mean free path of the diffusing gas molecules [12]. This diffusion mechanism is prominent in mesoporous systems, which have pore diameters smaller than the mean free path of a gas molecule. Thus, the interaction between gas molecule and pore wall is very important than the molecule-molecule interaction.

Knudsen number, Kn is a dimensionless number defined as the ratio of the mean free path of gas molecules to pore diameter [13]. The value is given by $Kn = \lambda/D_p$, where λ (m) being the mean free path of a gas molecule and D_p (m) is the pore diameter. When $\lambda \gg D_p$, the collision inside the narrow pore occurs more frequently between diffusing gas molecules and pore walls than with each other. Knudsen diffusion dominates at $Kn \gg 1$, and the permeance (Q_K) is described by following Eq. 1-7:

$$Q_K = \frac{\varepsilon D_p}{\tau L}\left(\frac{8}{9\pi MRT}\right)^{0.5} \tag{1-7}$$

where ε is the porosity of the membrane, D_p is the pore diameter, τ is the tortuosity, L (m) is mean membrane thickness, R (J.mol^{-1}.K^{-1}) is the gas constant, T (K) is the temperature, and M (g.mol^{-1}) is the molecular weight of the diffusing gas.

Since the driving force for transport is the partial pressure of the gas species, Knudsen transport can occur either by concentration gradients or by pressure gradients. The relative permeation rate of each component is inversely proportional to the square root of its molecular weight. The gas selectivity ($\alpha_{A/B}$) of Knudsen diffusion can be calculated with the square root of the ratio of respective molecular weights (M) of two molecules as shown in Eq. 1-8 [14]:

$$\alpha_{A/B} = \sqrt{\frac{M_B}{M_A}} \tag{1-8}$$

For example, in the case of O_2 and N_2, the permeance of smaller but heavier O_2 is slower than N_2 by the factor $(28/32)^{1/2} = 0.94$. Hence, separation through Knudsen diffusion exhibits low selectivity since it's only allow separation of gases with huge differences in their molecular weights. In spite of that, the gas fluxes through the membrane are considerably high.

1.2.3. Surface diffusion

Gas molecules can interact with the surface, adsorb on surface sites and be mobiles on the surface. In surface diffusion mechanism, the diffusing species are considered to be adsorbed on the surface and transport across the surface by hopping between the potential minima produced on the pore surface [15]. The membrane selectively adsorbed molecules with larger polarity and molecular weight on their surface [16]. The transport of non-selectively adsorbed species can be blocked by the adsorbed species on the membranes pores by controlling the size of accessible space across the pores [16]. This hindrance effect typically occurred when the pore size is between 2 to 3 molecular diameters of the adsorbed species. Since the diffusing gas molecules bound on the membrane surface may be released to be the gaseous state when their sorption energy is lower than their kinetic energy. Accordingly, depending on the sorption energy of the gas molecules, the surface diffusion is favourable at relatively low temperatures. In order to employ surface diffusion as an effective separation mechanism, it is necessary to maintain sufficient physical adsorption, and thus the separation should be operated below 300°C, while the membrane pore diameters should be smaller than 6 nm [17].

The surface diffusion permeances can be described by the following expression (Eq. 1-9):

$$Q_{SD} = Q_0 \exp\left(\frac{-\Delta H_a - \Delta E_{SD}}{RT}\right) \text{ with } Q_0 = \frac{\rho K_0 D_0}{L} \quad (1\text{-}9)$$

where ΔH_a (J.mol^{-1}) is the enthalpy of adsorption, ΔE_{SD} (J.mol^{-1}) is the energy barrier for molecule movement to the other adsorption site, R (J.mol^{-1}.K^{-1}) is the gas constant, ρ (kg.m^{-3}) is density of gas molecule, T (K) is the absolute temperature, K_0 (Pa^{-1}) is an adsorption equilibrium constant, D_0 is movement of molecules and L (m) is the thickness of the membrane.

1.2.4. Capillary condensation

Capillary condensation is a process in a porous medium where multilayer adsorption from a vapour proceeds to the point where pore spaces are filled with the condensed liquid. In porous system, at the temperature below the critical temperature point of the diffusing gas, the increase of pressure first leads to multilayer adsorption until finally all pores are filled with liquid [18]. A unique aspect of the capillary condensation is that, unlike regular condensation, vapour condensation occurs below saturation vapour pressure, P_{sat}, of a pure liquid. When the pore spaces become completely filled with the condensed liquid, the permeances through the membrane is completely restricted for the gaseous species which are insoluble in the condensed liquid. This separation mechanism seems to be effective due to high fluxes and selectivity. However, a condensable component is essentially required for an effective separation which

restricts its applicability range due to the temperature and pressure range needed for capillary condensation.

1.2.5. Molecular sieving and activated diffusion

Molecular sieving is a mechanism whereby different molecules are separated because of their different size. Molecular sieving can be used to separate molecules when the kinetic diameters of molecules are almost identical to the pore sizes of membranes. Based on this mechanism, the separation is caused by passage of smaller molecules of a gas mixture through the pores while the larger molecules are obstructed. This mechanism exhibits high selectivity and permeability for the smaller component of a gas mixture. However, a very fine-tuning of the membrane pore sizes is necessary for efficient separation [19].

The activated gas transport mechanism is one of the most characteristic properties in microporous membranes, which results in very high separation factors at high temperatures. It has been found that the permeance (Q_{MS}) through microporous materials increases as a function of temperature [20] as given by Eq. 1-10.

$$Q_{MS} = Q_0 \exp\left(-\frac{E_a}{RT}\right) \tag{1-10}$$

where Q_o (mol·m^{-2}·s^{-1}·Pa^{-1}) is pre-exponential factor, E_a (J.mol^{-1}) is an apparent activation energy, R (J.mol^{-1}.K^{-1}) is gas constant, and T (K) is temperature. For an active diffusion to occur, the temperature should be high enough to overcome energy barriers to atomic motion. Table 1-1 shows apparent activation energies of gas permeation in the polymer-derived amorphous SiOC and SiC membranes in comparison with those in amorphous silica (SiO$_2$) membranes fabricated by the chemical vapour deposition method [21].

1.2.6. Solution diffusion

In the solution-diffusion model, transport occurs only by diffusion. The fluid that needs to be transported must first be dissolved in the membrane. Solution-diffusion model based on the assumption that the chemical potential of the feed and permeates are in equilibrium with the adjacent membrane surfaces such that suitable expressions for the chemical potential in the fluid and membrane phases can be equated at the solution-membrane interface. This assumption is well known for dense or nonporous membranes which do not have natural pores for gas diffusion using other mechanisms as described above. Gases are soluble in the membrane matrix to a certain extent. The separation in the membrane takes place due to differences in solubility and diffusivity of gases [13]. The solution-diffusion model has postulated three

consecutive steps for gas transport: 1) sorption of gas molecule into the high-pressure side of the membrane, 2) diffusion of the gas through the membrane, and 3) desorption of the gas molecule at the low-pressure side of the membrane. When diffusion through the membrane takes place in the form of ions and electron or as atoms, the molecules first dissociate after adsorption and recombine after diffusing through the membrane.

The following Eq. 1.11 is commonly used to rationalize the properties of gas permeation membranes.

$$J_i = \frac{P_i^{G}\left(p_{i_o} - p_{i_l}\right)}{L} \tag{1-11}$$

where P_i^{G} (mol. m^{-1}.s^{-1}.Pa^{-1}) is permeability coefficient, $p_{io} - p_{il}$ (Pa) is pressure difference across the membrane and L (m) is membrane thickness.

This mechanism also widely applied for the separation in dense organic membrane and polymer membrane. Compared to porous membrane, the solution diffusion mechanism exhibits relatively high selectivity but with low fluxes.

Table 1-1. Apparent Activation Energies of Gas Permeations in Polymer-derived Amorphous Si(O)C Membranes, and CVD-derived Amorphous silica (SiO$_2$) Membranes [21].

Membrane	Permeation Temperature (°C)	Activation energy (kJ.mol^{-1})		References
		He	H$_2$	
SiOC[1]	10-550	7-13	7-15	[22]
SiOC[2]	77-200	9.8-15.4	16.3-16.7	[23]
SiC[1]	300-500	2.7	1.2	[24]
	500-600	9.4	6.0	[25]
SiC[3]	300-500	0.6	0.09	[26]
	500-600	1.2	0.3	
SiC[4]	25-250	5.7	5.2	[26]
SiO$_2$[5]	450-800	-	37	[27]
SiO$_2$[6]	200-650	-	6-25	[28]
SiO$_2$[7]	100-600	9.8	14.8	[29]
SiO$_2$[8]	100-600	8.1	16.8	[30]

[1]PCS, [2]PDS, [2]PDS, [3]PCS-[SiH$_2$Cl$_2$-C$_2$H$_2$ (CVI)], [4]PCS-PVS polymer blend, [5]SiCl$_4$-H$_2$O (CVD), [6,7]Si(OC$_2$H$_5$)$_4$-O$_2$ (CVD), and [8] Si(OCH$_3$)$_4$-O$_2$ (CVD)

1.3. Synthesis of microporous ceramic membranes for gas separation

Porous ceramic membranes needs multi-layered construction with graded porosity: Macroporous support, mesoporous intermediate layer and active molecular-sieving layer (top microporous layer) as illustrated in Figure 1-3. The macroporous support is the most porous part of the membrane and provides mechanical strength while minimizing mass transfer resistance. Then, to minimize the defects of top microporous ceramic membrane and to control overall porosity, mesoporous layer is developed on the tubular macroporous supports. The pore opening of the mesoporous membranes (few nm) avoids infiltration of the microporous ceramic into the pores of support, minimizing the effective thickness of the microporous membrane layer. The following describes the fabrication techniques of ceramics available for porosity controlling in multi-layer construction of porous ceramic membrane.
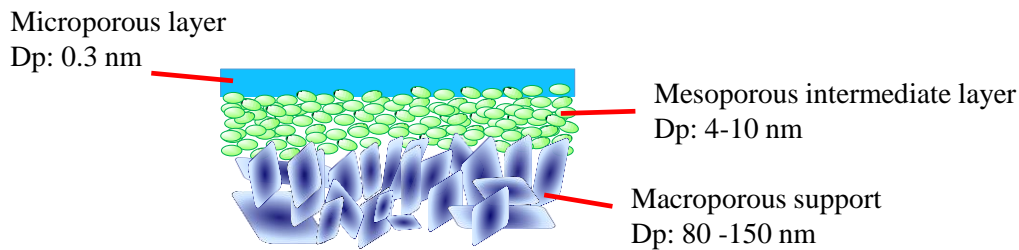
Figure 1-3. Schematic diagram of multi-layered construction of porous ceramic membranes with graded porosity.

1.3.1. Macroporous ceramics

Macroporous ceramic materials with pore size ranging from 400 nm to 4mm and porosity within the range of 20-97% have been produced and found widespread technological application, such as in molten metal filtration, catalysis, refractory insulation and hot gas filtration in various industrial processes [31]. These applications employ the unique properties achieved through integration of macropores into solid ceramics. The main processing routes available for fabrication of highly porous macroporous ceramics can be classified into replica, sacrificial template and direct forming methods, as shown in Fig. 1-4.

The replica method is frequently employed in the fabrication of macroporous ceramics having open cell walls and high volume porosity with interconnected large pores. In replica technique, a synthetic template, e.g. a polymer foam, is immersed into a ceramic suspension to impregnate the templates, followed by removal of excess suspension to allow the formation of thin ceramic coating on the surface of polymer foam [32]. Prior to sintering at higher

temperature, dry ceramic-impregnated templates must be pyrolyzed at slow heating rates to maintain the gradual decomposition and diffusion of the polymeric material. [33,34]. Although this process is well established in industry e.g; metal filtration and diesel engine exhaust filters, there are drawbacks concerning the final mechanical strength of the porous ceramics and variation in pore sizes [34-36]. During pyrolysis of the polymer foam, cracked and hollow cavities remain in the struts, which reduces the compressive strength of the final material [37]. In addition, the minimum pore size of this method is also limited to 200 μm [38].
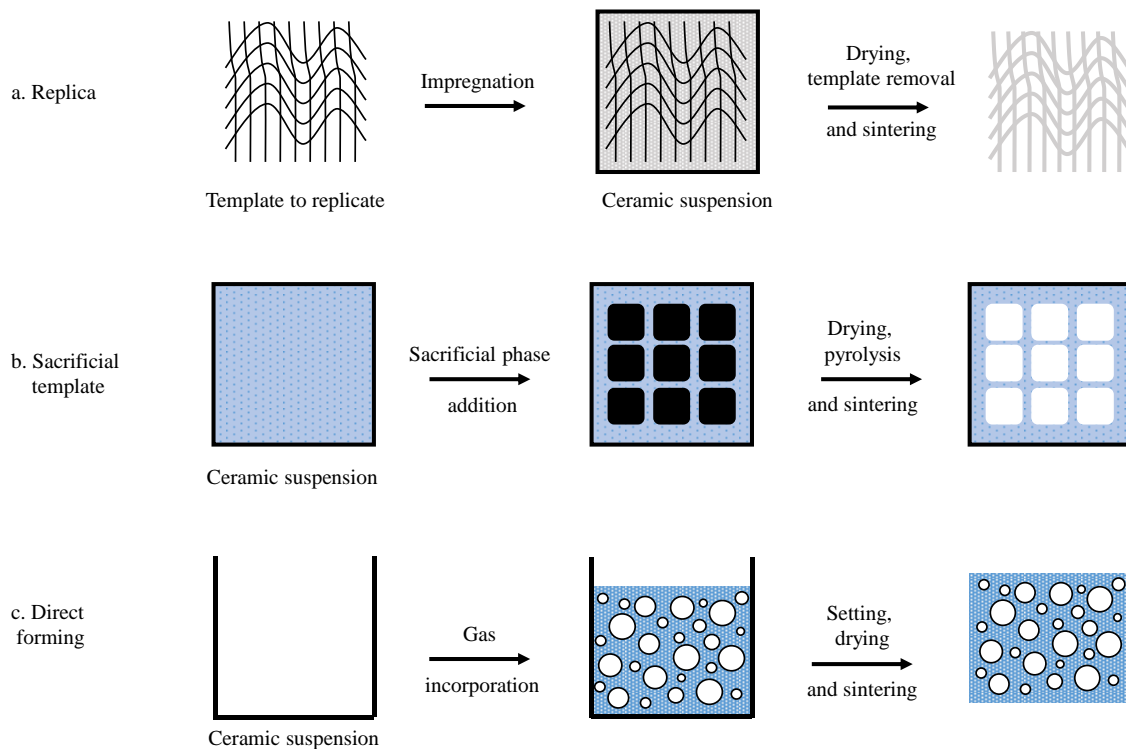
Fig. 1-4. Scheme of three processing routes for the fabrication of macroporous ceramics

The sacrificial template method typically consists of the preparation of a dual-phase composite involving a continuous matrix of a ceramic particles and initially homogenous distribution of dispersed sacrificial template (pore forming agents) which subsequently removed for pore formation. This method produces porous materials features a negative replica of the original sacrificial template. The frequently used pore forming agents includes polymer beads [39,40] and freeze dried liquids [41,42]. Through the appropriate choice of the sacrificial template, this method offers the flexibility to tailor the porosity, pore size distribution and pore morphology of the final ceramics. However, this method may expend a vast amount of time to removing the sacrificial template which leads to cracking and deformation of the material due to

induce stresses [33].

In direct foaming methods, porous materials are fabricated by incorporating air into a suspension or liquid media, which is subsequently set in order to preserve the structure of air bubbles created. Typically, the consolidated foams are afterwards sintered at high temperatures to obtain high-strength porous ceramics. However, generally the large pores are produced in the final porous ceramics due to thermodynamic instability of foam which typically consolidate in order to reduce the total Gibbs free energy of the system. So, this method depends on the use of surfactants or particles as a foam stabiliser to preserve the porous structure. This technique is relatively cheap and offers the simplest route for fabricating highly porous ceramics materials composed of dense pore walls, above 95% porosity. However, compared to replicate method, the porosity yielded by this method is generally less open, resulting in lower permeability and relatively higher strength [31].

1.3.2. Mesoporous ceramics

The synthesis of mesoporous materials since the first discovery in the early 1990's has expanded enormously. Generally, mesoporous ceramics can be prepared by using soft template method [43, 44] and hard template method [44, 45] as depicted in Figure 1-5.

In soft template method, the formation of organized organic-inorganic hybrids proceeds via self-assembly of surfactants or block copolymers with inorganic precursors or nanoparticles. The organic materials used as a template or structure directing agent (SDA) plays a crucial role to generate porosity within the building blocks, leading to mesostructured composites. The mesoporous inorganic materials could be obtained by subsequent removal of organic material by heat-treatment in air. Low molecular weight surfactants (e.g., cetyl-trimethylammonium bromide) were first employed in this soft template method, and mesostructured aluminosilicates with amorphous structures have been successfully synthesized [46]. In addition, mesostructured carbons with various pore sizes and pore structures, and transition metal oxides can be synthesized using the soft template method [47-51].

In hard template method, inorganic precursors are called into pre-synthesized hard template mesoporous silica or colloidal spheres, which are subsequently removed by etching with hydrofluoric acid (HF) or sodium hydroxide (NaOH), or heat-treatment under air. Hard template method is used to increase the crystallization temperature while maintaining the ordered mesostructure of mesoporous metal oxides. The hard template method allows the fabrication of thermally stable and highly crystalline mesostructured materials with various wall compositions. However, this method is time consuming and the removal of the silica template using hydrofluoric acid (HF), is quite tedious and dangerous.

(a) Soft-template method

Micelle   Mesoporous product

(b) Hard-template method

Mesoporous template   Mesoporous replica
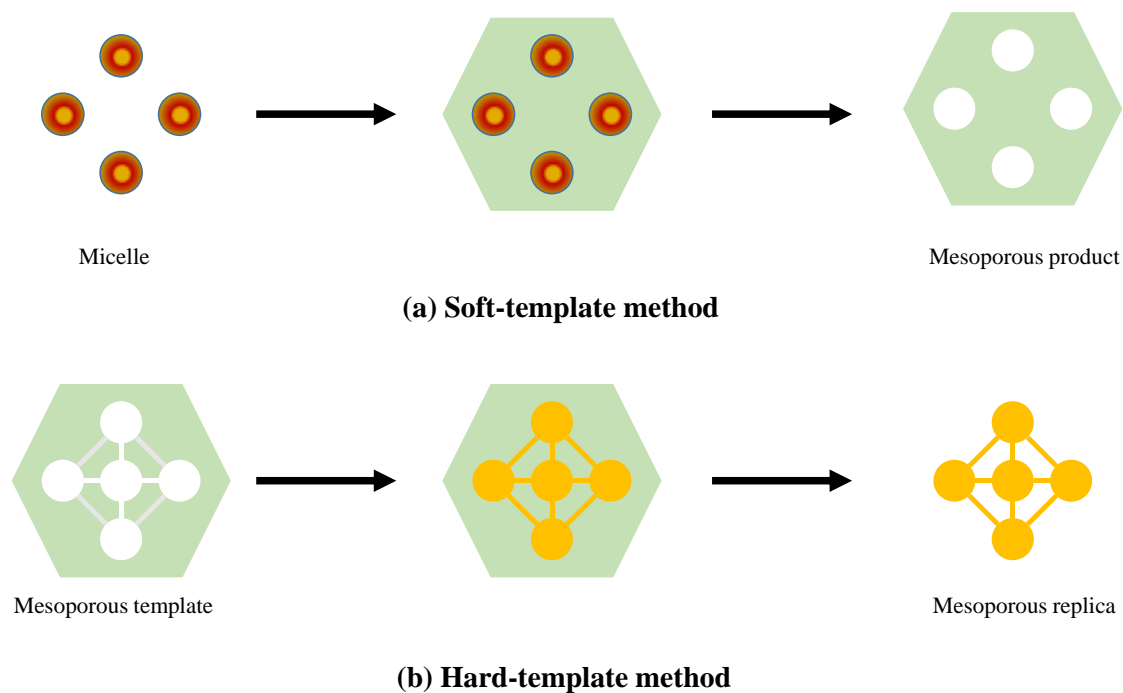
Fig. 1-5. Fabrication of mesoporous materials using a) soft-template method and b) hard-template method.

1.3.3. Microporous ceramics

Amorphous silica is the most widely studied material for microporous ceramics membranes. Microporous amorphous silica contains intrinsic defects formed as the six-membered ring of tetrahedral SiO_4 unit with a diameter of approximately 0.3 nm, suitable for hydrogen (0.289 nm) separation from larger gas molecules such as CO_2, CO, and CH_4. Microporous amorphous silica holds several advantages compared to Pd-based membranes for hydrogen separation membranes especially in terms of chemical stability and cost. As shown in Fig. 1-6, microporous amorphous silica-based membranes synthesized by the sol-gel and/or chemical vapour deposition (CVD) methods have been shown to be very effective for H_2 selective separation [27, 52-54].

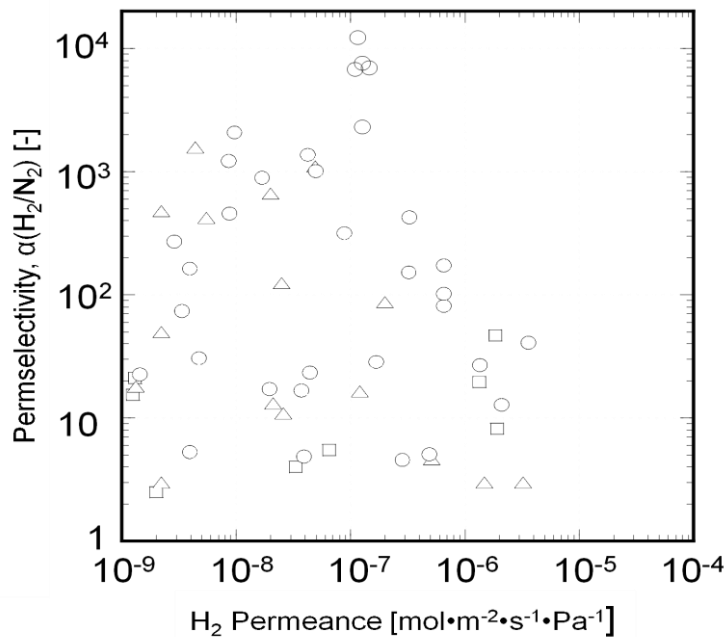Figure 1-6. H$_2$ permselectivity of the metal-organic precursor-derived amorphous silica-based membranes. The literature data measured under dry condition at permeation temperatures ranging from □: 300°C $\leqq$ T $<$ 400°C, ∆: 400°C $\leqq$ T $<$ 500°C, and ○: 500°C $\leqq$ T $\leqq$ 600°C were taken from ref. [10].

In addition to the membrane performance under dry condition at high-temperatures, considerable emphases have been given to enhance the H$_2$ permselectivity of microporous amorphous silica membranes. Naturally, silica is hydrophilic due to the existence of the surface silanol (Si-OH) groups. Owing to that, the decrease of H$_2$ flux through microporous amorphous silica membrane has been reported under humid environments resulting from the micropore blocking due to the presence of adsorbed water at low temperatures [55]. Thus, in order to mitigate this problem, it is essential to enhance the hydrostability of silica by making it hydrophobic. This can be achieved with the introduction of organic groups on silica surfaces, since it has a distinctive effect in terms of increasing the hydrophobicity of silica [56,57]. Such improvement on the performance of silica membrane with hydrophobicity enhancement could be observed where H$_2$ permeances was increased with temperature [58] and found suitable for application in humid process streams [59] below the thermal decomposition temperature of the organic groups (approximately, 250°C) .

The following section briefly described the fabrication routes applied for microporous amorphous silica-based membranes.

(1) Sol-gel processing route

Sol–gel processing is a wet chemical technique used for the fabrication of microporous amorphous silica-based membranes which offers reaction tunability and choice of precursors. This technique is attractive since the pore size of the membrane can be desirably controlled. The preparation of membrane using sol-gel processing can be achieved using two routes i.e. colloidal route or a polymer route. In the colloidal route, the synthesis takes place in an aqueous medium where the colloids remain isolated due to electrostatic repulsion. On the other hand, in polymeric route, the synthesis occurs in an alcoholic medium where sol particles, due to their small size, remain separated in solution. The typical sol-gel process is shown in Fig. 1-7. In both cases, the condensation reactions plays an important role for the formation of colloids or clusters during sol stage, which later on interact to form a sol. The sol formed then coated on the membrane support to form a colloidal gel or polymer gel, respectively. In most cases, the fabrication of inorganic membrane can be done by dip-coating followed by subsequent thermal treatment. This two routes yield nano-sized particles from which porous materials can be synthesized. The polymeric route yields particles essential for fabricating microporous silica-based materials and membranes. The silica-based membrane fabricated using sol-gel processing shows good gas separation properties for various gas mixtures, such as H_2/CH_4, H_2/N_2 and H_2/CO_2 [59-64].
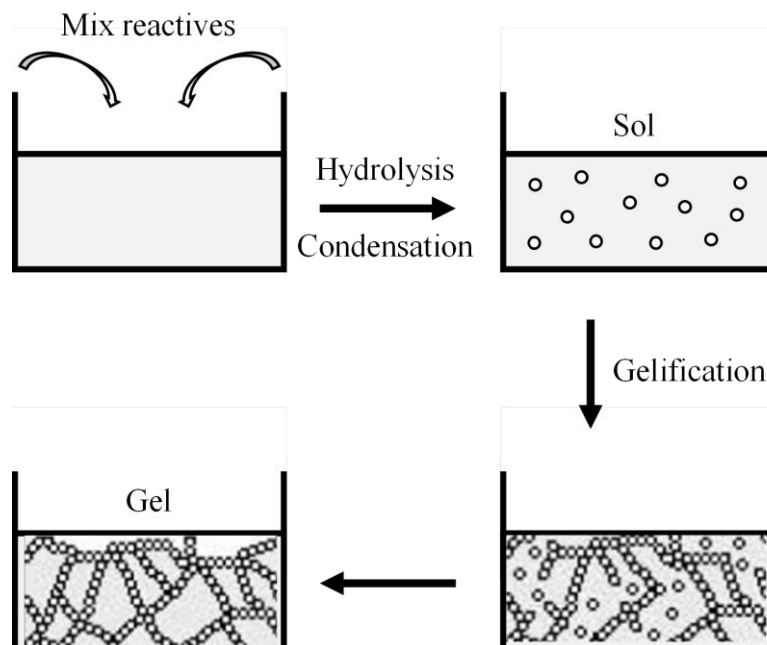

Fig. 1-7. Illustration of typical sol gel-process.

(2) Chemical vapour deposition (CVD) and/or chemical vapour infiltration (CVI) route

Amorphous silica membranes by the chemical vapour deposition (CVD) and/or the chemical vapour infiltration (CVI) can be formed by the decomposition of gas phase precursors inside the micro- and mesopores of the intermediate mesoporous layer placed on the macroporous support surface, thereby blocking the pore diameter to molecular dimensions [27,28,65-76]. A layer of the same or different compound is deposited on a membrane surface through chemical reactions taking place in a vapour phase surrounding the substrate. The CVD system consists of a mixture of reactive and carrier gas, a heated reaction chamber, and a system for the treatment and disposal of exhaust gases. Gas mixture flowed to a reaction chamber and heated to a desired temperature where solid film is deposited on the surface. The schematic diagram of chemical vapour deposition is shown in Fig. 1-8.

The volatile by-products produced from CVD system which contains various hazardous components and particles need to be treated before exhaust to the atmosphere, which typically removed by gas flow through the reaction chamber. In most cases, CVD method produced membranes with lower permeances and higher selectivity.
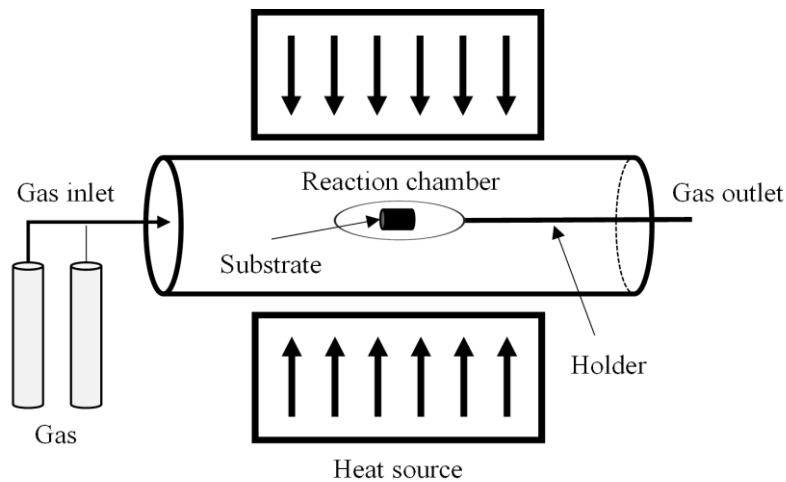
Fig. 1-8. Schematic diagram of CVD technique.

As one of the modified CVD techniques, Nomura et al. [77] synthesized amorphous silica membranes on γ-Al$_2$O$_3$ (average pore sizes of 4 and 13 nm)-coated α-Al$_2$O$_3$ by using the counter diffusion chemical vapour deposition (CDCVD) technique. In CDCVD, a membrane is synthesized at the contact point of the source and reaction gases inside the intermediate layer, as shown in Fig. 1-9. The pore size, pore filling homogeneity, silica density gradient within the mesoporous intermediate layer, and effective membrane thickness can be controlled by changing the reactants and reaction conditions. The deposition rate of the membrane

automatically decreases when the diffusion rates of the source and reaction gases decrease with the deposition. Therefore, the amorphous silica membrane synthesized by CDCVD exhibits high H_2 permeances [30, 78].
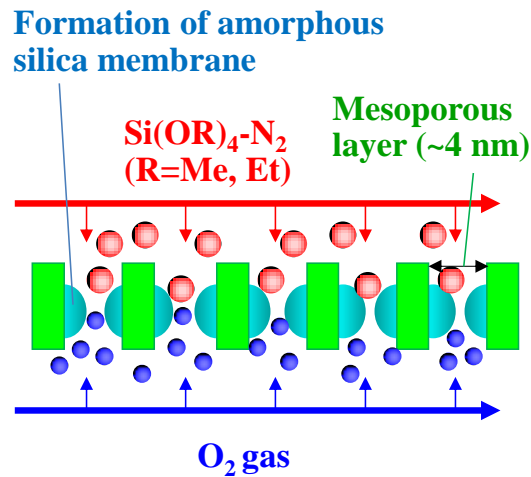

Fig. 1-9. Formation mechanism of amorphous silica membrane in counter diffusion chemical vapour deposition (CDCVD).

1.4. Novel porous structure controlling through polymer-derived ceramics (PDCs) route

Polymer-derived ceramics (PDCs) route is originally studied on the chemical formation of silicon (Si)-based non-oxide ceramics such as silicon carbide (SiC) and silicon nitride (Si_3N_4) by thermal conversion of silicon (Si)-based polymers such as polycarbosilane (PCS), polysilazanes (PSZ) [79-82]. This route provides some potential advantages in controlling purity and the materials can be easily shaped in various forms i.e. fibers, layers or bulk composite materials by applying processing techniques established in the plastic industry. The polymeric nature of the precursors offers the use of processing techniques otherwise not feasible for ceramics, where PDCs route represents an alternative to conventional powder-technology based ceramic processing (powder metallurgy route). Preceramic polymers have been used for obtaining a wide variety of complex ceramic structures for energy-related applications, including coatings, fibers, bulk materials, and composites [82]. In addition, PDCs route also offer possibilities for in-situ controlling micro-/meso-porous structure development suitable for constructing the multi-layered porous membranes to develop high-performance hydrogen separation membranes.

1.4.1. Macroporous structure controlling

Scientific interest in polymer-derived cellular ceramics has demonstrated the potential for obtaining macroporous materials with uniform, graded, or hierarchical pore systems [83-85]. The partial sintering of powder compacts or mixtures is the most straightforward route and frequently employed for the preparation of macroporous ceramics [86,87]. However, this method often results in low porosity yields (<60%) and the options to alter the pore size distribution is rather limited [88,89]. It has been recently demonstrated that polymer-derived ceramics route can be used to produce highly macroporous structures (foams, membranes, components with hierarchical porosity) of various compositions and morphologies [81,84]. The highly ordered macroporous ceramic powders, e.g silicon carbonitride [90] (SiCN) and silicon carbonitride (SiC) [91] have been successfully obtained from preceramic polymers using sacrificial templates. Recently, Sung *et al.* successfully fabricated highly macroporous silicon carbonitride (SiCN) and silicon carbide (SiC) ceramic monoliths possessing pore diameters ranging from 50 nm to 10 mm by the pyrolysis of polysilazane-filled packed beds of polystyrene (PS) or silica (SiO_2) spheres [92]. Vakifahmetoglu *et al.* produced highly porous macro-cellular SiCN foams by pyrolysis of liquid polysilazane and a physical blowing agent blending mixture in a single-step process [93]. The illustration of ordered macroporous ceramics is shown in Fig. 1-10.
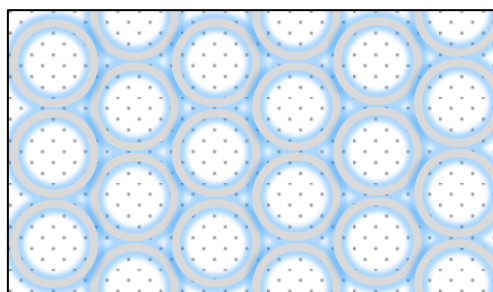

Fig. 1-10. Illustration image of ordered macroporous materials.

1.4.2. Meso-/Micro-porous structure controlling

The generation of Meso- [94-96] and Micro-[10,26, 94, 97-104] porous ceramic compounds from preceramic polymers has gained increasing scientific interest in recent years. Meso-/Micro-porosities in PDCs are generally produced during the thermal conversion of polymer precursor to ceramics [105,106]. Both the evolution of gaseous by-products as a result of the decomposition of organic groups leads to the meso-/micro-porosity formation. Moreover, structure rearrangements at the molecular scale within the three dimensional amorphous network lead to the formation of an intrinsic microporosity [107]. However, the microporosity is

thermally unstable and further increase in temperature results in a closing of micropores, mainly due to the viscous flow processes governed by the reduction in surface energy [108]. As a typical example, polysiloxane-derived microporous amorphous siliconoxycarbide (Si-O-C) compounds exhibit a significant reduction in microporosity starting from 450°C and almost complete collapse of the micropores at temperatures above 700°C [106].

On the other hand, non-oxide PDCs such as polysilazane-derived binary silicon carbide (Si-C), silicon nitride (Si-N) and ternary silicon carbonitride (Si-C-N) exhibit improved resistance against oxidation and creep at elevated temperatures [10]. As a result, the fabrication of these types of microporous non-oxide ceramics for a variety of fields, including catalysis and membrane applications, has gained increasing attention [104,105,109]. Dismukes and co-workers [105] reported on a variety of methods to generate microporous polysilazane-derived non-oxide ceramics, including the controlled thermal decomposition in a reactive atmosphere, in this case, ammonia (NH_3), the use of inert, sub-micrometer sized fillers, the formation of metal- or cermet-ceramic composites from polysilazane-stabilized metal colloids, or the thermal conversion of polysilazane mixed with metal-organic compounds. Using these methods, materials with specific surface areas > 500 m^2 g^{-1} and micropore volumes > 0.2 cm^3 g^{-1} were generated. A further increase in thermal stability of the micropore structure, i.e. the shift of the pore collapse onset towards higher temperatures, was reported by chemical modification of the preceramic polymer, e.g. by the addition of Ni [103,109], or by using a reactive gas atmosphere such as NH_3 during thermal decomposition [104].

Owing to the straightforward method of generating and controlling their micropore structure, ternary Si-(O)-C [10,23,26,97-100,110], microporous PDC-based Si-N [111], Si-C-N [95, 102], and quaternary silicon boron carbonitride (Si-B-C-N) [96,101] have been investigated as selective layer structures in membrane systems. In addition to the non-oxide systems, polymer-derived amorphous silica (Si-O) membranes have been also reported [94,112]. Iwamoto and co-workers [94] reported on the formation of both meso- and micro-porous amorphous silica by the controlled pyrolysis and subsequent heat treatment of polyorganosilazanes, and hydrogen perm-selective amorphous silica membranes were successfully synthesized. Moreover, perhydropolysilazane (PHPS) was also converted to hydrogen perm-selective amorphous silica membrane by the plasma oxidation at room temperature [112].

1.5. Objectives of present research

As briefly reviewed in the previous section, the PDCs route offers several advantages in fabrication of porous ceramics. The meso- and micropore formation could be achieved by altering the polymeric precursor. The alkyl substituent bonded to each silicon atom acted as

"sacrificial templates" for the meso- and micropores. However, for the synthesis of amorphous silica material, the effects of alkyl chain length and the number of alkyl substituents on the porous structure formation have not been understood comprehensively.

The first objective of this study is to synthesize amorphous silica with controlled porosity in the micro/meso-pore ranges through PDCs route. As an alkyl substituent-free starting polymer, perhydropolysilazane (PHPS) was selected, and was chemically modified with various alcohols to afford alkoxy group-functionalized PHPS. The alkoxy group introduced to PHPS was acted as sacrificial template for porosity formation during conversion of polymer into amorphous silica by heat treatment in air.

The second objective of this study is to clarify the *in-situ* porosity formation of the chemically modified PHPS-derived amorphous silica. The alkoxy group-functionalized PHPSs were converted to amorphous silica-based inorganic-organic hybrids using room temperature oxidation technique, followed by thermal conversion to amorphous silica in air. To understand the porosity development within the silica materials, evaluation of the gaseous species formed *in-situ* during thermal treatment was performed using simultaneous thermogravimetry-mass spectrometry (TG-MS) analysis.

The third objective of this study is to synthesize amorphous silica with an enhanced hydrophobicity. As mentioned in the section 1.3.3, the hydrophobicity improvement has been achieved by introducing alkyl groups to some extent. However, the hydrophobicity of micro-and mesoporous amorphous silica-based organic-inorganic hybrid materials has not been recognized well. In this study, the alkoxy group-functionalized amorphous silica-based inorganic-organic hybrid materials were synthesized from PHPS chemically modified with alcohols and alcohol derivatives using room temperature oxidation technique. The relationships between the chain length of the alkoxy groups, density of Si-OH groups, mean mesopore size and the water vapour sorption behaviour were intensively studied and discussed.

References

[1]   H. Mei, C. Li, S. Ji, H. Liu, Chem. Eng. Sci., 62 (2007) 4294 – 4303.

[2]   A. Basile, L. Paturzo, Catal. Today, 67 (2001) 55-64.

[3]   I.E.A., "Moving to a hydrogen economy: dreams and realities", IEA/SLT (2003) 5.

[4]   K. Li, "Ceramic Membranes for Separation and Reaction", Wiley, Chichester, (2007).

[5]   K. Akamatsu, S. Nakao, J. Jpn. Petrol. Inst., 54 (2011) 287-297.

[6]   C. A. Scholes, K. H. Smith, S. E. Kentish, G. W. Stevens , Int. J. Greenhouse Gas Control, 4 (2010) 739-755.

[7]   P. Bernardo, E. Drioli, G. Golemme, Ind. Eng. Chem. Res., 48 (2009) 4638-4663.

[8]   K. Maeda, K. Domen, J. Phys. Chem, 111 (2007) 7851-7861.

[9]   S. Sagyu et al., Private communication (1969).

[10]   Y. Iwamoto, J. Ceram. Soc. Jpn., 115 (2007) 947-954.

[11]   G. Saracco, V. Specchia, Catal. Rev. Sci. Eng., 36 (1994) 305–384.

[12]   M. Knudsen, Ann. Phys., 28 (1909) 75.

[13]   R.R. Bhave, "Inorganic Membranes: Synthesis, Characteristics and Applications", Van Nostrand Reinhold, New York, (1991).

[14]   R.J.R. Uhlhorn, K. Keizer, A.J. Burggraaf, J. Membr. Sci., 46 (1989) 225–241.

[15]   A.J. Burggraaf, J. Membr. Sci., 155 (1999) 45.

[16]   M.B. Rao, S. Sircar, J. Membr. Sci., 110 (1996) 109-118.

[17]   R.J.R. Uhlhorn, "Ceramic membranes for gas separation: synthesis and gas transport properties", University of Twente, Enschede, (1990).

[18]   A.J. Burggraaf, L. Cot, "Fundamentals of Inorganic Membrane Science and Technology", Elsevier (1996).

[19]   M.B. Rao, S. Sircar J Membr Sci 85 (1993) 253-264.

[20]   R.S.A. de Lange, K. Keizer, A.J. Burggraaf, J. Membr. Sci., 104 (1995) 81-100.

[21]   Y. Iwamoto, "5.7. Membranes", in Polymer Derived Ceramics ed. by P. Colombo, R. Riedel, G. D Sorarù and H.-J. Keebe, DEStech Publications, Inc., PA, USA (2010) pp. 396-402.

[22]   Z. Li, K. Kusakabe, S. Morooka, J. Membr. Sci. 118 (1996) 159-168.

[23]   L.L. Lee, D.S. Tsai, J. Am. Ceram. Soc., 82 (1999) 2796-2800.

[24]   T. Nagano, K. Sato, T. Saito, Y. Iwamoto, J. Ceram. Soc. Japan, 114 (2006) 533-538.

[25]   T. Nagano, K. Sato, T. Saito, Y. Iwamoto, Soft. Materials, 4 (2007) 109-122

[26]   R.A. Wach, M. Sugimoto, M. Yoshikawa, J. Am. Ceram. Soc., 90 (2007) 275-278.

[27]   M. Tsapatsis, S. Kim, S.W. Nam, G.R. Gavalas, Ind. Eng. Chem. Res., 30 (1991) 2152.

[28]   S. Morooka, S. Yan, K. Kusakabe, Y. Akiyama, Membrane Sci., 101 (1995) 89-98.

[29]   D. Lee, L. Zhang, S.T. Oyama, S. Niu, R.F. Saraf, J. Membr. Sci., 231 (2004) 117-126.

[30] T. Nagano, S. Fujisaki, K. Sato, K. Hataya, Y. Iwamoto, M. Nomura, S-I, Nakao, J. Am. Ceram. Soc. 91 (2008) 71-76.

[31] A.R. Studart, U.T. Gozenbach, E. Tervoort, L.J. Gauckler, J. Am. Ceram. Soc., 89 (2006) 1771-1789.

[32] P. Colombo. Phil. Trans. R. Soc. A, 364 (2006) 109-124.

[33] O. Lyckfeldt, J.M.F. Ferreira. J. Eur. Ceram. Soc., 18 (1998) 131-140.

[34] J. Saggio-Woyansky, C. E. Scott, W. P. Minnear, Am. Ceram. Soc. Bull., 71 (1992) 1674-1682.

[35] J.T. Richardson, Y. Peng, D. Remue, Appl. Catal., 204 (2000) 19-32.

[36] G.F.A. Acosta, E.A.H. Castillejos, R.J.M. Almanza, V.A. Flores, Metall. Mater. Trans. B, 26 (1995) 159-171.

[37] L.J. Gibson, M.F. Ashby, "Cellular Solids: Structure and Properties", 2nd edition, Cambridge University Press, Cambridge, (1997).

[38] F.F. Lange, K.T. Miller, Adv. Ceram. Mater., 2 (1987) 827-831.

[39] F. Tang, H. Fudouzi, T. Uchikoshi, Y. Sakka. J. Eur. Ceram. Soc., 24 (2004) 341-344.

[40] Y. Kim, Y. Jin, Y. Chun, I. Song, H. Kim. Scripta Mat., 53 (2005) 921-925.

[41] K. Araki, J.W. Halloran., J. Am. Ceram. Soc., 87 (2004) 1859-1863.

[42] H. Kim, J.C. Knowles, H. Kim., J. Biomed. Mater. Res. A, 72 (2005) 136-145.

[43] N. Pal, A. Bhaumik, Adv. Coll. Inter. Sci., 189-190 (2013) 21-41.

[44] Y. Ye, C. Jo, I. Jeong, J. Lee, Nanoscale, 5 (2013) 4584-4605.

[45] S. Bernard, P. Miele, New. J. Chem., 38 (2014) 1923-1931.

[46] C.T. Kresge, M.E. Leonowicz, W.J. Roth, J. C. Vartuli, J.S. Beck, Nature, 359 (1992) 710-712.

[47] C. Liang, S. Dai, J. Am. Chem. Soc., 128 (2006) 5316–5317.

[48] Y. Huang, H. Cai, T. Yu, F. Zhang, F. Zhang, Y. Meng, D. Gu, Y. Wan, X. Sun, B. Tu, D. Zhao, Angew. Chem, 46 (2007) 1089-1093.

[49] Q. Huo, D. I. Margolese, U. Ciesla, P. Feng, T.E. Gier, P. Sieger, R. Leon, P.M. Petroff, F. Schuth, G.D. Stucky, Nature, 368 (1994) 317-321.

[50] Q. Huo, D.I. Margolese, U. Ciesla, D.G. Demuth, P.Feng, T.E. Gier, P. Sieger, A. Firouzi, B. F. Chmelka, Chem. Mater., 6 (1994) 1176-1191.

[51] D. Gu, F. Schuth, Chem. Soc. Rev., 43 (2014) 313-344.

[52] R.M. De Vos, H. Verweij, Science, 279 (1998) 1710-1711.

[53] L.J.P. Van Den Broeke, W.J.W. Bakker, F. Kapteijn, J.A. Moulijn, AIChE J., 45 (1999) 976-985.

[54] J. Sekulic, M.W.J. Luiten, J.E. Ten Elshof, N.E. Benes, K. Keizer, Desalination, 148 (2002) 19–23.

[55] K. Tanaka, Y. Sakata, Membrane 36 (2011) 113-121.

[56] J. Mecinovic, P. W. Snyder, K. A. Mirica, S. Bai, E.T. Mack, R.L. Kwant, D.T. Moustakas, A. Heroux, G. M. Whitesides, J Am. Chem. Soc., 133 (2011) 14017-26.

[57] N. Gokulakrishnan, T. Karbowiak, J. P Bellat, L. Vonna, M. Saada, J. L Paillaud, M. Soulard, J. Patarin, J. Parmentier, Colloids Surf., A 421 (2013) 34-43.

[58] S. Giessler, L. Jordan, J.C.D. da Costa , G.Q. Lu, Sep. Porif. Technol., 32 (2003) 255-264.

[59] R. M. de Vos, W. F. Maier, H. Verweij, J. Membr. Sci., 158 (1999) 277-288.

[60] M. Asaeda, Y. Oki, T. Manabe, "Preparation of Porous Silica Membranes for Separation of Inorganic Gaseous Mixtures at High Temperature", Subarea C: Science and Technology for Energy Conversion, September (1993) pp. 253-258.

[61] M. Asaeda, M. Kashimoto, "Sol-Gel Derived Silica Membranes for Separation of Hydrogen at High Temperature-Separation Performance and Stability against Steam", in the Proceedings of 5th ICM (1998) pp.172-175.

[62] M. Kanezashi, M. Asaeda, J. Membr. Sci., 271 (2006) 86-93.

[63] R. Igi, T. Yoshioka, Y. H. Ikuhara, Y. Iwamoto, T. Tsuru, J. Am. Ceram. Soc., 91 (2008) 2975-2981.

[64] T. Tsuru, R. Igi, M. Kanezashi, T. Yoshioka, S. Fujisaki, Y. Iwamoto, AIChE Journal, 57 (2011) 618-629.

[65] G. R. Gavalas, C. E. Megiris, S. W. Nam, Chem. Eng. Sci., 44 (1989) 1829-1835.

[66] C. E. Megiris, J. H. E. Glezer, Chem. Eng. Sci., 147 (1992) 3925-3934.

[67] H. Y. Ha, S. W. Nam, S. A. Hong, W. K. Lee, J. Membr. Sci., 85 (1993) 279-290.

[68] J. C. S. Wu, H. Sabol, G. W. Smith, D. L. Flowers, P. K. T. Liu, J. Membr. Sci., 96 (1994) 275-287.

[69] C. L. Lin, D. L. Flowers, P. K. T. Liu, J. Membr. Sci., 92 (1994) 45-58.

[70] M. Tsapatsis, G. Gavalas, J. Membr. Sci., 87 (1994) 281-296.

[71] S. Jiang, Y. Yan, G. R. Gavalas, J. Membr. Sci., 103 (1995) 211-218.

[72] B. Sea, M. Watanabe, K. Kusakabe, S. Morooka, S. Kim, Gas. Sep. Purif., 10 (1996) 187-195.

[73] H. A. Ha, J. S. Lee, S. W. Nam, I. W. Kim, S. A. Hong, J.Mater. Sci., 16 (1997) 1023-1026.

[74] B. Sea, E. Soewito, M. Watanabe, K. Kusakabe, S. Morooka, S. Kim, Ind.Eng. Chem. Res., 37 (1998) 2502-2508.

[75] G. Hwang, K. Onuki, S. Shimizu, H. Ohya, J. Membr. Sci., 162, (1999) 83-90.

[76] D. Lee, S. T. Oyama, J. Membr. Sci., 210 (2002) 291-306.

[77] M. Nomura, H. Aida, S. Gopalakrishnan, T. Sugawara S-I. Nakao, S. Yamazaki, T. Inada,

Y. Iwamoto, Desalination, 193 (2006) 1-7.

[78]   K. Miyajima, T. Eda, B. N. Nair, S. Honda, Y. Iwamoto, J. Ceram. Soc. Japan, 121 (2013) 992-998.

[79]   E. Kroke, Y.-L. Li, C. Konetschny, E. Lecomte, C. Fasel, R. Riedel, Mater. Sci. Eng. R., 26 (2000) 97-199.

[80]   R. Riedel, G. Mera, R. Hauser, A. Klonczynski, J. Ceram. Soc. Jpn., 114 (2006) 425-444.

[81]   P. Colombo, R. Riedel, G.D. Sorarù, H.-J. Kleebe, "Polymer derived Ceramics: From Nano-Structure to Applications", in, DEStech Publications, Inc., Lancaster (2010).

[82]   T. Konegger, J. Torrey, O. Flores, T. Fey, B. Ceron-Nicolat, G. Motz, F. Scheffler, M. Scheffler, P. Greil, R. K. Bordia, "Ceramics for Sustainable Energy Technologies with a Focus on Polymer Derived Ceramics", Springer, India (2014) pp. 501-533.

[83]   J. Zeschky, F. Goetz-Neunhoeffer, J. Neubauer, S. H. J. Lo, B. Kummer, M. Scheffler, P. Greil, Compos. Sci. Technol., 63 (2003) 2361-2370.

[84]   P. Colombo, J. Eur. Ceram. Soc., 28 (2008) 1389-1395.

[85]   P. Colombo, C. Vakifahmetoglu, S. Costacurta, J. Mater. Sci., 45 (2010) 5425-5455.

[86]   R.W. Rice, "Porosity of ceramics", Marcel Dekker Inc. NewYork, (1998) pp. 539.

[87]   M. Scheffler, P. Colombo, "Cellular ceramics: Structure, Manufacturing, Properties and Applications" Weinheim, Wiley-VCH, (2005) pp. 645.

[88]   S. Shan, J. Yang, J. Gao, W. Zhang, Z. Jin, R. Janssen, T. Ohji. J. Am. Ceram. Soc., 88 (2005) 2594-2596.

[89]   I.H. Arita, V.M. Castano, D.S. Wilkinson. J. Mater. Sci.-Mater. M., 6 (1995) 19-23.

[90]   H. Wang, S.-Y. Zheng, X.-D Li, D.-P. Kim, Microporous Mesoporous Mater., 80 (2005) 357-362.

[91]   I.-K. Sung, S.-B. Yoon, J.-S. Yu, D.-P. Kim, Chem. Commun., (2002) 1480-1481.

[92]   I.-K. Sung, M.M. Christian, D.-P. Kim, P.J.A. Kenis, Adv. Func. Mater. 15 (2005) 357-362.

[93]   C. Vakifahmetoglu, I. Menapace, A. Hirsch, L. Biasetto, R. Hauser , R. Riedel , P. Colombo, Ceram. Inter., 35 (2009) 3281-3290.

[94]   Y. Iwamoto, K. Sato, T. Kato, T. Inada, Y. Kubo, J. Eur. Ceram. Soc., 25 (2005) 257-264.

[95]   K. W. Völger, R. Hauser, E. Kroke, R. Riedel, Y. H. Ikuhara, Y. Iwamoto, J. Ceram. Soc. Jpn., 114 (2006) 567-570.

[96]   R. Hauser, S. Nahar-Borchard, R. Riedel, Y. H. Ikuhara, Y. Iwamoto, J. Ceram. Soc. Jpn., 114 (2006) 524-528.

[97]   K. Kusakabe, Z. Y. Li, H. Maeda, S. Morooka, J. Membr. Sci., 103 (1995) 175-180.

[98]   H.M. Williams, E.A. Dawson, P.A. Barnes, B. Rand, R.M.D. Brydson, A.R. Brough, , J.

Mater. Chem., 12 (2002) 3754-3760.

[99] H. Suda, H. Yamauchi, Y. Uchimaru, I. Fujiwara, K. Haraya, Desalination, 193 (2006) 252-255.

[100] B. Elyassi, M. Sahimi, T. T. Tsotsis, J. Membr. Sci., 288 (2007) 290-297.

[101] R.M. Prasad, Y. Iwamoto, R. Riedel, A. Gurlo, Adv. Eng. Mater., 12 (2010) 522-528

[102] Y. Jüttke, H. Richter, I. Voigt, R.M. Prasad, M.S. Bazarjani, A. Gurlo, R. Riedel, , Chem. Eng. Trans., 32 (2013) 1891-1896.

[103] M.S. Bazarjani, M.M. Müller, H.J. Kleebe, Y. Jüttke, I. Voigt, M.B. Yazdi, L. Alff, R. Riedel, A. Gurlo, ACS Appl. Mater. Inter., 6 (2014) 12270-12278.

[104] C. Schitco, M.S. Bazarjani, R. Riedel, A. Gurlo, J. Mater. Chem. A, 3 (2015) 805-818.

[105] J.P. Dismukes, J.W. Johnson, J.S. Bradley, J.M. Millar, Chem. Mater., 9 (1997) 699-706.

[106] H. Schmidt, D. Koch, G. Grathwohl, P. Colombo, J. Am. Ceram. Soc., 84 (2001) 2252-2255.

[107] M. Wilhelm, C. Soltmann, D. Koch, G. Grathwohl, J. Eur. Ceram. Soc., 25 (2005) 271-276.

[108] P. E. Sánchez-Jiménez, J.A. Downs, R. Raj, J. Am. Ceram. Soc., 93 (2010) 2567-2570.

[109] M.S. Bazarjani, H.J. Kleebe, M.M. Müller, C. Fasel, M.B. Yazdi, A. Gurlo, R. Riedel, Chem. Mater., 23 (2011) 4112-4123.

[110] B. Elyassi, M. Sahimi, T. T. Tsotsis, J. Membr. Sci., 316 (2008) 73-79.

[111] K. Miyajima, T. Eda, H. Ohta, Y. Ando, Y. Iwamoto, Ceram. Trans., 213 (2010) 87-94.

[112] K. Miyajima, T. Eda, B. N. Nair, Y. Iwamoto, J. Membr. Sci., 421-422 (2012) 124-130.

Chapter 2. Synthesis of microporous amorphous silica from perhydropolysilazane chemically modified with alcohol derivatives

2.1. Introduction

The advancement of ceramic processing in the last few decades has resulted in various types of ceramic materials being synthesized and characterized for wide range application. The organometallic precursor route is one of the ceramic processing methods that received considerable attention since it offers several advantages as compared to conventional powder processing methods such as purity control, compositional homogeneity in the ceramic end-product and lower processing temperatures in ceramic preparation [1-3]. In addition, this route offers opportunities to synthesize advanced silicon-based non-oxide ceramics such as silicon nitride (Si_3N_4)-based ceramics, and there have been several reports on the synthesis of Si_3N_4-based ceramics from polysilazanes [4,5]. Especially, perhydropolysilazane (PHPS) has some advantages in high purity and high ceramic yield [6]. Furthermore, PHPS contains many reactive Si-H and N-H groups which can react with chemical modifiers to yield novel ternary or quaternary Si-based non-oxide ceramics [7-10]. In addition, PHPS has also received considerable attention as a favourable precursor for synthesizing pure silica because PHPS can be easily oxidized to yield pure silica with high ceramic yield [11]. Recently, Iwamoto et al. [12] has reported an approach in controlling the micro- and meso-porous structure formation by using organo-substituted polysilazane precursor. The organo-substituted group acted as a "sacrificial template" during polymer to ceramic conversion by heat treatment in air, which leading to the micro- and meso-porous structure formation [12]. Owing to this feature, PHPS to silica conversion has a potential to be used in the fabrication of microporous amorphous silica-based membranes for gas separation [12,13].

In this study, as sacrificial templates for microporous structure formation, alkoxy groups were introduced to PHPS by using an alcohol derivative as a chemical modifier, and converted the polymer into amorphous silica by heat treatment in air. The chemical modification reaction of PHPS with various alcohol derivatives was studied using ^{1}H-NMR and FT-IR spectroscopic analyses. Then, the polymer/ceramic conversion behaviours, and the relationships between the chemical structure of alkoxy groups, thermal properties of the chemically modified PHPSs and the microporous structure formation were studied and discussed from a viewpoint to develop a novel method for synthesizing microporous amorphous silica-based materials through polymer precursor route.

2.2. Experimental procedures

2.2.1. Precursor synthesis

Commercially available perhydropolysilazanes (PHPS, Type NN110, 20% xylene solution, AZ Electronic Materials, Japan) was used as a starting polymer. In this study, alcohol derivatives of methanol (CH_3OH), i-propanol ($CH(CH_3)_2OH$), n-pentanol (n-$C_5H_{11}OH$) and n-decanol (n-$C_{10}H_{21}OH$) were used for the chemical modification of PHPS. The reaction between as-received PHPS and the alcohol derivative was carried out under dry argon (Ar) atmosphere using Schlenk techniques [14]. The molar ratio of the reactants was set at the Si of PHPS/ROH molar ratio of 4/1. Then, the molar ratios of 8/1 and 2/1 were further investigated for the PHPS chemically modified with n-$C_{10}H_{21}OH$.

To the xylene solution of as-received PHPS, the alcohol derivative was added drop wise under magnetic stirring at room temperature. After the addition was completed, the mixture was heating at 120°C and refluxed for 1h under flowing Ar. After cooling down to room temperature, the xylene was removed from the reaction mixture under vacuum to give an alcohol adduct as viscous liquid.

2.2.2. Oxidative crosslinking and pyrolysis

To control the vigorous oxidation reaction in air, the thermal conversion process in this study was divided into the following two steps; 1) Polymer precursor was cured by heating at 270°C in air to promote oxidative crosslinking with a heating rate of 100°C/h and dwell time of 1h in an alumina tube furnace. After cooling down to room temperature, the cross-linked polymer was obtained as white solid. 2) The cross-linked polymer precursor was ground to a fine powder using a mortar and pestle, then pyrolyzed in a furnace under flowing air by heating from room temperature to 600°C in 6 h, maintaining the temperature at 600°C for an additional 1h, and finally cooling down to room temperature to give amorphous silica as white powders.

2.2.3. Characterization

Fourier transform infrared (FT-IR) spectra of the polymers, cross-linked and pyrolyzed products were recorded on KBr pellets in the wavenumber range of 4000-400 cm^{-1} (Model FT/IR-4200 IF, Jasco, Japan). ^1H nuclear magnetic resonance (NMR) spectra were recorded for the polymers in $CDCl_3$ solution at room temperature (Model AV400N, Bruker, USA). Thermogravimetric analysis (TGA) was performed on the cross-linked precursors up to 1000°C at a heating rate of 100°C/h under air flowing (Model TG8120, Rigaku, Tokyo, Japan).

The pore size distribution of the pyrolyzed samples was measured using nitrogen (N_2) sorption technique with the relative pressure of the N_2 gas ranging from 0 to 0.99 (Model Belsorp Max, BEL Japan Inc., Osaka, Japan). The micropores ($r_{pore} < 2.0$ nm) and mesopores

(2.0 nm $\leqq r_{pore} <$ 50 nm) of the polymer-derived amorphous silica were characterized by the SF [15] and BJH [16] methods, respectively.

2.3. Results and discussion

2.3.1. Chemical structure of precursors

The chemical structure of the polymer precursors were studied by the FT-IR spectroscopic analysis. As shown in Fig. 2-1(a), as-received PHPS exhibits absorption bands at 3400 cm^{-1} (vN-H), 2150 cm^{-1} (vSi-H), 1180 cm^{-1} (δN-H) and 840-1020 cm^{-1} (δSi-N-Si) [4,17]. The spectra of PHPS modified with CH$_3$OH [Fig. 2-1(b)] and that with i-C$_3$H$_7$OH [Fig. 2-1(c)] presents additional absorption bands at 2950-2850 cm^{-1} (vC-H), 1450 cm^{-1} (δCH$_3$), and 1090 cm^{-1} (vSi-OR) [18]. However, the intensity of the absorption bands due to the C-H bond in the spectrum of PHPS modified with i-C$_3$H$_7$OH is relatively weak, suggesting that the reactivity of i-C$_3$H$_7$OH to PHPS was not sufficient due to the steric hindrance caused by the bulky secondary alkyl group. On the other hand, in the spectra of PHPS modified with n-C$_5$H$_{11}$OH [Fig. 2-1(d)] and that with n-C$_{10}$H$_{21}$OH [Fig. 2-1(e)], the intensity of the absorption bands due to the C-H bond remarkably increased.
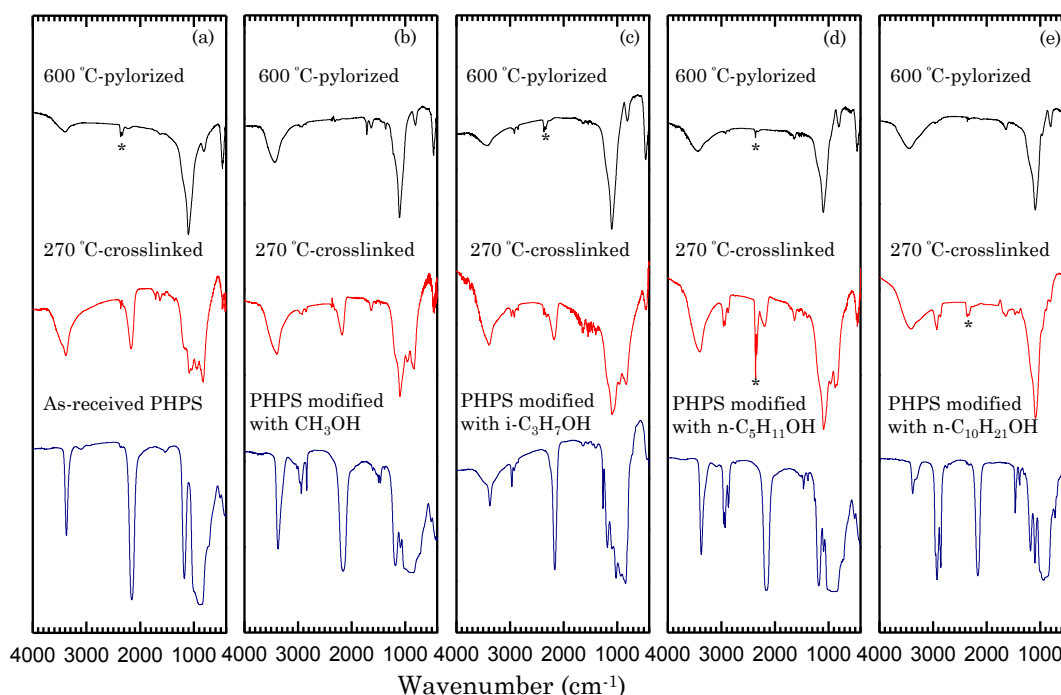
Fig. 2-1. IR spectra of polymer state and thermally treated in air of (a) PHPS, (b) PHPS modified with CH$_3$OH, (c) PHPS modified with CH(CH$_3$)$_2$OH, (d) PHPS modified with C$_5$H$_{11}$OH and (c) PHPS modified with C$_{10}$H$_{21}$OH (* indicating background, absorption due to CO$_2$).

The reaction between PHPS and alcohol derivative was further studied by ^{1}H-NMR spectroscopic analysis. As a typical result, the ^{1}H-NMR spectrum of PHPS chemically modified with n-$C_{10}H_{21}OH$ is shown and compared with those of starting compounds, as-received PHPS and n-$C_{10}H_{21}OH$ in Fig. 2-2(a). The peak assignment for the n-$C_{10}H_{21}OH$ is also shown in this figure [9]. As-received PHPS presents broad peaks at 5.2-4.5, 4.3 and 1.8-1.0 ppm assigned to SiH/SiH_2, SiH_3 and NH, respectively [8,9]. The ^{1}H-NMR spectrum of the PHPS chemically modified with n-$C_{10}H_{21}OH$ mainly consists of the peaks of PHPS and the $C_{10}H_{21}$ group. However, the peak of an alcoholic proton (H_E) at 1.5 ppm disappears and the peaks of the n-$C_{10}H_{21}$ group are broader in comparison with those in the spectrum of the starting n-$C_{10}H_{21}OH$, indicating the influence of the polymer network of PHPS. As shown in Fig. 2-2(b), with increasing the Si/n-$C_{10}H_{21}OH$ molar ratio from 8/1 to 2/1, the intensity of the broad peak centred at 4.74 ppm within the peaks due to SiH/SiH_2 decreased, and at the Si/n-$C_{10}H_{21}OH$ molar ratio = 2/1, a new signal at 4.69 ppm begins to appear as a small shoulder on the peak of $HSiN_3/H_2SiN_2$ (marked by an arrow), which indicating the formation of $HSiON_2$ groups [8-9]. These FT-IR and ^{1}H-NMR spectroscopic data indicate that the alcohol derivative mainly reacted with H_2SiN_2 groups of PHPS to form RO-$SiHN_2$ groups [9].
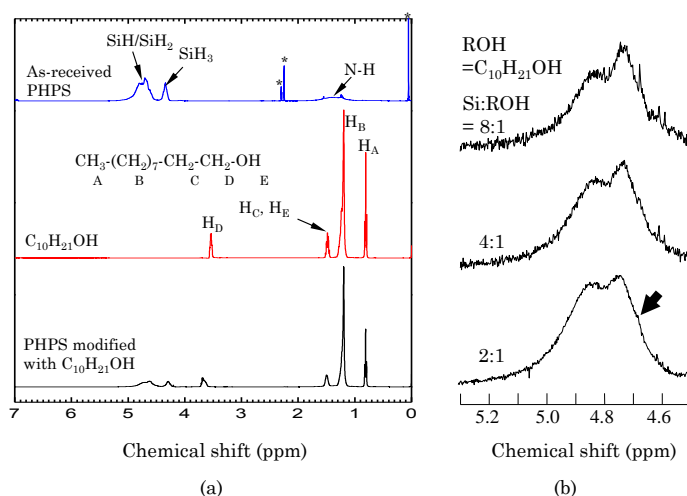

Fig. 2-2. ^{1}H NMR spectra of (a) as-received PHPS, $C_{10}H_{21}OH$, and PHPS modified with $C_{10}H_{21}OH$, (b) PHPS modified with $C_{10}H_{21}OH$ at the Si/R-OH molar ratio = 8/1, 4/1 and 2/1 (* indicating noise peak).

2.3.2. Cross-linked polymers and their conversion into amorphous silica powders

The 270°C-crosslinked PHPS exhibits a new absorption band at 3400 cm^{-1} (Si-OH) [18], and decreases in intensity of the absorption bands due to the Si-H (2150 cm^{-1}), N-H (1180 cm^{-1}) and Si-N-Si (840-1020 cm^{-1}). After pyrolysis at 600°C in air, the absorption bands derived from

PHPS completely disappeared and the Si-O absorption band intensity increased, indicating that PHPS was fully oxidized and converted into amorphous silica [Fig. 2-1(a)]. In the spectra of the 270°C-crosslinked samples derived from chemically modified PHPSs, the C-H absorption bands were still detected as minor peaks, then completely disappeared after the pyrolysis at 600°C in air. Thus, all the cross-linked samples were successfully converted into amorphous silica [Figs. 2-1(b)-(e)].

To study the cross-linked polymer/amorphous silica conversion process in more detail, thermogravimetric (TG) analysis was performed. The results were summarized and shown in Fig. 2-3. The weight change of the cross-linked PHPS could not be clearly observed in the temperature range below 200°C. Then, a significant weight gain was observed as much as 13% at 200 to 500°C. Above 600°C, the sample weight slightly decreased, and the total weight gain measured at 1000°C was 12 %.

The 270°C-crosslinked samples derived from PHPSs having alkoxy groups show a slight weight loss below 200°C, then the similar weight gain was for the samples derived from PHPS having CH_3O groups and that having $i-C_3H_7O$ groups. However, the weight gain at 200 to 500°C decreased consistently with the number of carbon atoms of the alkoxy groups introduced to PHPS. Upon heating to 600°C, the 270°C-crosslinked PHPS modified with $n-C_5H_{11}OH$ showed a total weight loss of 12 %, and the higher weight loss of 31 % was observed for the sample derived from PHPS modified with $n-C_{10}H_{21}OH$ (Fig. 2-3).
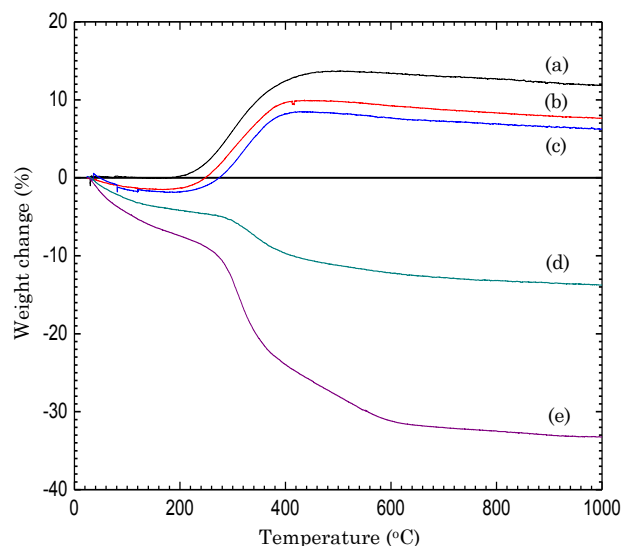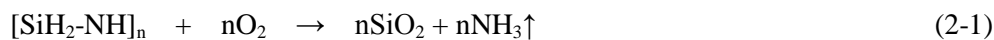

Fig. 2-3. TGA of 270°C-crosslinked sample derived from (a) as-received PHPS, and PHPS modified with (b) CH_3OH, (c) $CH(CH_3)_2OH$, (d) $C_5H_{11}OH$, and (e) $C_{10}H_{21}OH$ from room temperature to 1000°C at a heating rate of 100°C/h under flowing air.

The weight gain observed for the cross-linked PHPS can be explained by the oxidation reactions like Eqs. (2-1) and (2-2), while one possible reason suggested for the slight weight loss above 600°C is the dehydration reaction shown in Eq. (2-3).

$$[SiH_2\text{-}NH]_n \ + \ nO_2 \ \rightarrow \ nSiO_2 + nNH_3\uparrow \qquad\qquad (2\text{-}1)$$

$$2 \equiv Si\text{-}H + \ O_2 \ \rightarrow \ 2 \equiv Si\text{-}OH \qquad\qquad (2\text{-}2)$$

$$2 \equiv Si\text{-}OH \rightarrow \ \equiv Si\text{-}O\text{-}Si \equiv \ + \ H_2O \qquad\qquad (2\text{-}3)$$

The weight loss below 200°C observed for the samples derived from chemically modified PHPS was partly due to the evaporation of solvent remained. As shown in Fig. 2-4, the weight loss at 200 to 500°C increased consistently with the number of $n\text{-}C_{10}H_{21}O$ groups by increasing the amount of $n\text{-}C_{10}H_{21}OH$ in the chemical modification of PHPS, i.e., $Si/n\text{-}C_{10}H_{21}OH$ molar ratio from 8/1 to 2/1. Thus, the significant weight loss observed for the samples derived from PHPS having $n\text{-}C_5H_{11}O$ groups and that having $n\text{-}C_{10}H_{21}O$ groups was mainly attributed to the decomposition and elimination of the alkoxy groups.
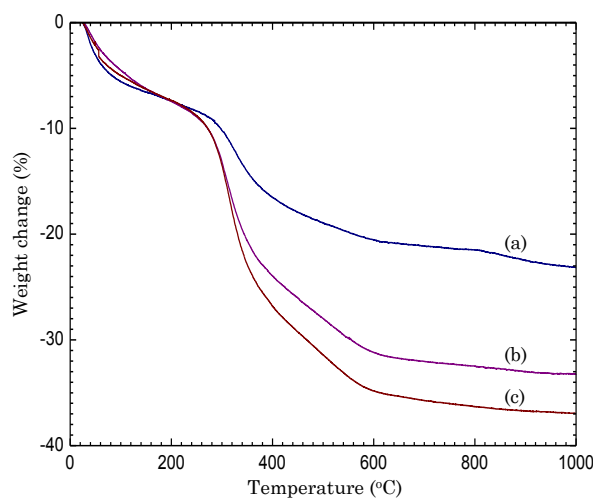

Fig. 2-4. TGA of 270°C-crosslinked PHPS modified with $C_{10}H_{21}OH$ at the Si/R-OH molar ratio of (a) 8/1, (b) 4/1, and (c) 2/1 from room temperature to 1000°C at a heating rate of 100°C/h under flowing air.

2.3.3. Porous structure of polymer-derived amorphous silica powders

The textural properties of the polymer-derived amorphous silica were studied by the N_2 physisorption at -196°C (77 K), and the adsorption/desorption isotherms are shown in Fig. 2-5. The PHPS-derived amorphous silica presents a type III isotherm in the IUPAC classification, indicating non-porous. The similar type III isotherm was observed for the amorphous silica

samples derived from PHPS having CH_3O groups and that having i-C_3H_7O groups.

On the other hand, the isotherm of amorphous silica derived from PHPS having n-$C_5H_{11}O$ groups presents a transitional type between typical type I and type IV without hysteresis loops. The N_2 uptake at the relative pressure lower than P/P_o= 0.2 reveals the micropore filling, while another slight up take at P/P_o=0.85 and above is thought to be due to the meso- and/or macro-porosity generated by agglomeration of the powdered sample. Thus, the isotherm of this sample is ascribed to type I-related microporous material.

The isotherm of amorphous silica derived from PHPS having n-$C_{10}H_{21}O$ groups also presents a similar transitional type, and the N_2 uptake below P/P_o=0.2 is remarkably increased.
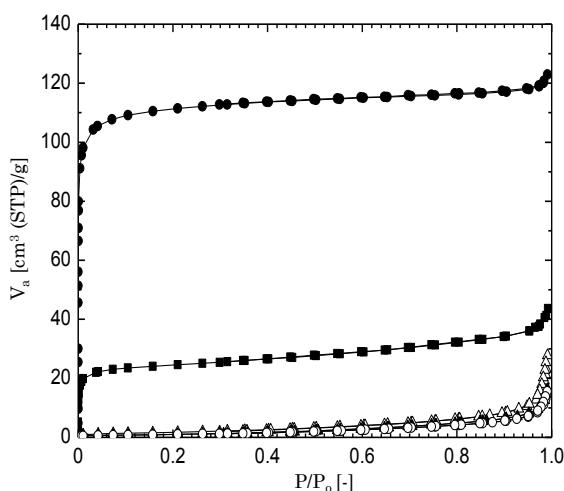
Fig. 2-5. Nitrogen sorption isotherm of 600ºC-pylorized sample derived from (a) as-received PHPS, and PHPS modified with (b) CH_3OH, (c) $CH(CH_3)_2OH$, (d) $C_5H_{11}OH$, and (e) $C_{10}H_{21}OH$.

Figure 2-6(a) shows the pore size distribution (PSD) curves obtained for the polymer-derived amorphous silica. The PSD curves for the micropores (r_{pore} < 2.0 nm) and those for mesopores (2.0 nm $\leqq$ r_{pore} < 50 nm) were characterized by the SF [15] and BJH [16] methods, respectively. The micropore volume of these samples are plotted as a function of number of carbon atoms in the alkoxy groups and shown in Fig. 2-6(b). Compared with the three kinds of non-porous amorphous silica samples, an apparent enhancement in the micropore volume can be observed while longer organic chain of alkoxy groups were introduced to PHPS. The PSD curve of amorphous silica derived from PHPS having n-$C_5H_{11}O$ groups was detected in the range of 0.43- 0.84 nm and peaked at 0.5 nm with micropore volume about 0.038 cm^3/g. By introducing n-$C_{10}H_{21}O$ groups, micropores having a size range of 0.43 – 1.3 nm were detected, and the PSD curve exhibited a peak top at 0.43 nm with the micropore volume about 0.173

cm^3/g. This micropore volume is highest among the five samples, and approximately four times higher than that derived from PHPS having n-C$_5$H$_{11}$O groups.
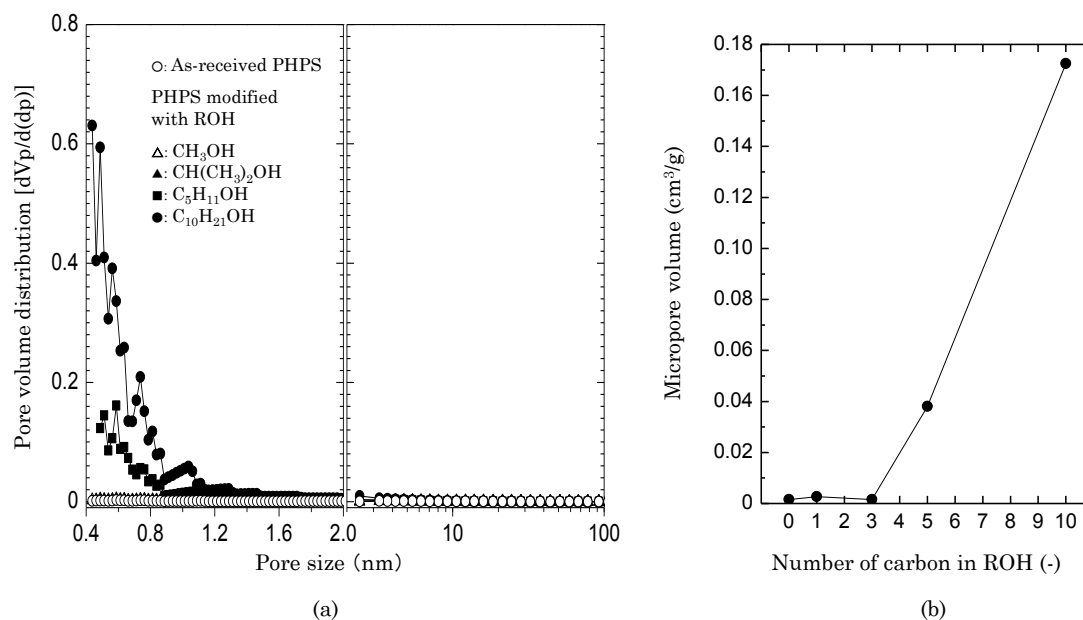

Fig. 2-6. Micro- and meso-porous structure of 600°C-pylorized samples evaluated by the nitrogen sorption analysis. (a) Pore size distribution and (b) Micropore volume as a function of the number of carbon in ROH used for the chemical modification of PHPS.

The effect of varying Si/ROH molar ratio in the PHPS chemical modification was further studied by using n-C$_{10}$H$_{21}$OH. The results are summarized and shown in Figs. 2-7 and 2-8. The amount of n-C$_{10}$H$_{21}$OH was reduced into half (8/1) and increased to double (2/1) while maintaining PHPS initial amount. The isotherms of all the samples presented the transitional type between the type I and type IV, and the N$_2$ uptake below P/P$_o$ = 0.2 increased consistently with the Si/ROH molar ratio. As a result, the highest N$_2$ uptake of 125 cm^3 (STP) g^{-1} was achieved at the Si/ROH molar ratio =2/1 (Fig. 2-7).
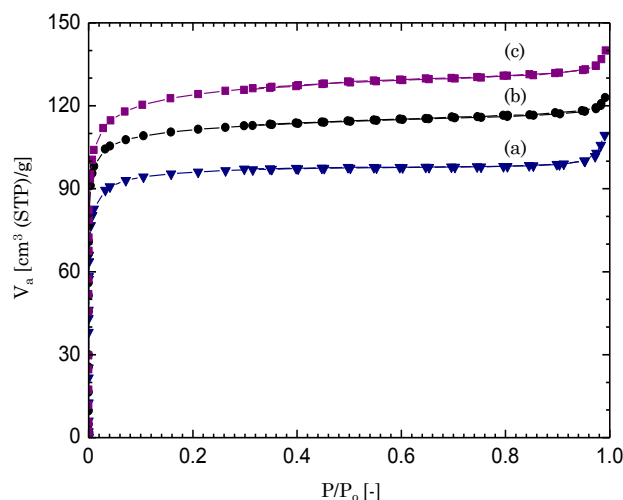
Fig. 2-7. Nitrogen sorption isotherm of 600°C-pylorized sample derived from PHPS modified with $C_{10}H_{21}OH$ at the Si/R-OH molar ratio of (a) 8/1, (b) 4/1, and (c) 2/1.

The PSD curves obtained for the three samples are shown in Fig. 2-8(a). By varying the molar ratio, the PSD curves located in the range of 0.43 – 1.3 nm are quite similar, and the height of the peak top at 0.43 nm apparently increased when the molar ratio increased to 2/1. As shown in Fig. 2-8(b), the resulting micropore volume increased linearly with the molar ratio, and reached 0.193 cm^3/g at the molar ratio = 2/1, while the specific surface area of this amorphous silica powder was measured to be 370 m^2/g.

However, both of the weight loss during pyrolysis and the resulting micropore volume of the pyrolyzed sample were not increased linearly with the amount of the n-$C_{10}H_{21}OH$ used for the chemical modification of PHPS. This could be due to the formations of the oligomers or monomers. As previously reported [9], during the chemical modification of PHPS with alcohol derivatives, Si-N bond cleavage of PHPS could be occurred to some extent, and the resulting by-products of the oligomers and/or monomers having the alkoxy groups were thought to be evaporated during the solvent removal under vacuum and/or oxidative crosslinking up to 270°C. The amount of the by-products was thought to be increased consistently with the amount of n-$C_{10}H_{21}OH$ used for the chemical modification of PHPS, which leading to the decrease in the efficiency of the micropore formation.
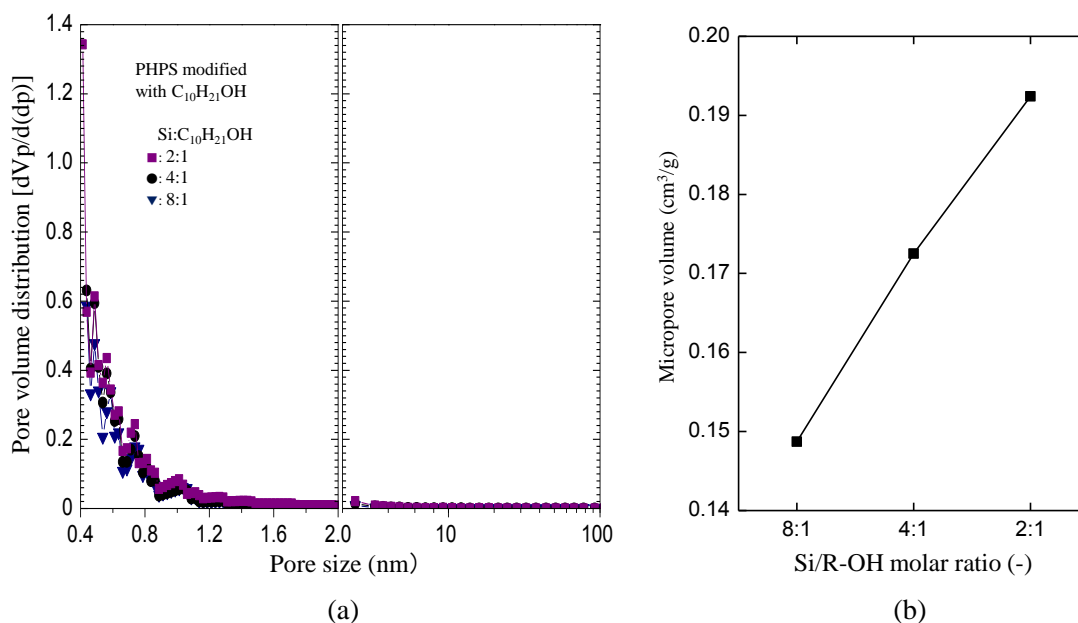
Fig. 2-8. Micro- and meso-pore size distribution of 600°C-pylorized samples derived from PHPS modified with $C_{10}H_{21}OH$ at the $Si/C_{10}H_{21}OH$ molar ratio of 8/1, 4/1, and 2/1. (a) Pore size distribution, and (b) Micropore volume as a function of the $Si/C_{10}H_{21}OH$ molar ratio used for the chemical modification of PHPS.

On the other hand, the alkoxy groups introduced to the polymer network of PHPS completely decomposed during the pyrolysis up to 600°C (Fig. 2-1), and the microporous structure development was found to be observed for the samples which exhibited the apparent weight loss at 200-500°C during the pyrolysis (Figs. 2-3 and 2-4). Moreover, the micropore volume was found to be increased consistently with the weight loss, and especially, n-$C_{10}H_{21}OH$ was found to be effective for the micropore formations. These results revealed that the thermal decomposition of the organic groups is essential for the microporous structure development of the polymer-derived amorphous silica investigated in this study.

The shape of the isotherms and the PSD curves characterized for the amorphous silica suggest some potential of the polymer route in this study as a novel method to synthesize super-microporous amorphous silica-based materials for energy application such as a highly efficient catalyst support and a gas separation membrane.

2.4. Conclusion

In this study, commercially available PHPS was chemically modified with alcohol derivative (ROH, R= CH_3, i-C_3H_7, n-C_5H_{11}, n-$C_{10}H_{21}$). The alkoxy group-functionalized PHPS was converted into amorphous silica powders by oxidative crosslinking at 270°C and

subsequent pyrolysis at 600°C in air. The results can be summarized as follows:

(1) FT-IR and ^{1}H-NMR spectroscopic analyses revealed that the alcohol derivative mainly reacted with H_2SiN_2 groups of PHPS to form $RO-SiHN_2$ groups.

(2) As-received PHPS and the alkoxy group-functionalized PHPS were successfully converted into amorphous silica by the two-step heat treatment in air.

(3) The results of pore size distribution analysis revealed that the microporosity of polymer-derived amorphous silica increased with the number of carbon atoms of ROH used as a chemical modifier for PHPS, and a significant increase in the micropore volume was observed for the amorphous silica when $n-C_{10}H_{21}OH$ was used as the chemical modifier.

(4) It was also found that the micropore volume could be enhanced with increasing the amount of $n-C_{10}H_{21}OH$ used for the chemical modification, and reached 0.193 cm^3/g at the molar ratio = 2/1.

(5) The micropore volume increased consistently with the weight loss detected at 200 to 500°C, and it was found to be essential for the microporous structure development that the thermal decomposition of the alkoxy groups introduced to PHPS.

(6) The textural properties of the polymer-derived amorphous silica suggested some potential of this polymer route to develop a novel method for synthesizing super-microporous amorphous silica-based materials.

References

[1]   R.W. Rice, Am. Ceram. Soc. Bull. 62 (1983) 889-892.

[2]   K.J. Wynne, R.W. Rice, Annu. Rev. Mater. Sci. 14 (1984) 297.

[3]   R. Riedel, W. Dressler, Ceram. Int. 22 (1996) 233.

[4]   D. Seyferth, C. Strohmann, N.R. Dando, A.J. Perrotta, Chem. Mater. 7 (1995) 2058.

[5]   E. Kroke, Y.-L. Li, C. Konetschny, E. Lecomte, C. Fasel, R. Riedel, Mater. Sci. Eng. R Reports 26 (2000) 97.

[6]   Funayama, M. Arai, Y. Tashiro, H. Aoki, T. Suzuki, K. Tamura, H. Kaya, H. Nishii, T. Isoda, J. Ceram. Soc. Japan 98 (1990) 104.

[7]   O. Funayama, T. Kato, Y. Tashiro, T. Isoda, J. Am. Ceram. Soc. 76 (1993) 717.

[8]   O. Funayama, Y. Tashiro, T. Aoki, T. Isoda, J. Ceram. Soc. Japan 102 (1994) 908.

[9]   Y. Iwamoto, K. Kikuta, S. Hirano, J. Mater. Res. 13 (1998) 353.

[10]   Y. Iwamoto, K. Kikuta, S. Hirano, J. Ceram. Soc. Japan 108 (2000) 350.

[11]   T. Kubo, H. Kozuka, J. Ceram. Soc. Japan 114 (2006) 517.

[12]   Y. Iwamoto, K. Sato, T. Kato, T. Inada, Y. Kubo, J. Eur. Ceram. Soc. 25 (2005) 257.

[13]   Y. Iwamoto, J. Ceram. Soc. Japan 115 (2007) 947.

[14]   D.F. Shriver, M.A. Drezdzon, The Manipulation of Air-Sensitive Compounds, (1986).

[15]   A. Saito, H.C. Foley, AIChE J. 37 (1991) 429.

[16]   E.P. Barrett, L.G. Joyner, P.P. Halenda, J. Am. Chem. Soc. 73 (1951) 373.

[17]   D. Seyferth, G.H. Wiseman, C. Prud'homme, J. Am. Ceram. Soc. 66 (1983) C13-C14.

[18]   K.R. Jennings, Org. Mass Spectrom. 26 (1991) 813.

Chapter 3. Polymer-derived amorphous silica-based inorganic-organic hybrids having alkoxy groups: intermediates for synthesizing microporous amorphous silica materials

3.1. Introduction

The use of chemical approaches in ceramic processing allowed a direct access to numerous types of ceramic materials that can be synthesized and characterized for a broad range of applications. The organometallic precursor route has received growing attention as an attractive ceramic processing method since it has inherent advantages over conventional powder processing methods such as purity control, compositional homogeneity in the ceramic final-product and lower processing temperatures in ceramic preparation [1-3]. Moreover, this route provides alternatives towards the synthesis of advanced silicon-based non-oxide ceramics such as silicon nitride (Si_3N_4)-based ceramics, particularly starting from polysilazanes as reported in several studies [4-6] Perhydropolysilazane (PHPS) has been extensively studied as a carbon free polymer precursor, that is readily oxidized to yield pure silica with a high ceramic yield, either by pyrolysis in air, [7] or by exposure to aqueous ammonia vapour at room temperature [8,9].

To date, micro- and meso-porous structures formation has been often discussed for the polymer-derived amorphous ceramics such as silicon nitride (Si-N), [10,11] silicon carbide (Si-C), [12-17] silicon carbonitride (Si-C-N), [18] quaternary Si-M-C-N (M=B, [19,20] Ni [21]), silicon oxycarbide (SiOC), [22-24] and silica (Si-O) [7,25,26]. During the crosslinking and subsequent high-temperature pyrolysis of polymer precursors, by-product gases such as CH_4, NH_3 and H_2 were detected [5,27], and the microporosity in the polymer-derived non-oxide amorphous ceramics could be assigned to the release of the small gaseous species formed in-situ [11,27].

Iwamoto *et al.* [7] reported an approach in controlling the micro- and meso-porous structure formation using organo-substituted polysilazane precursor, in which the organic moieties acted as a "sacrificial template" during polymer to ceramic conversion by heat treatment in air, thus allowing the micro- and meso-porous structure formation. Then, as discussed in Chapter 2, alkoxy group-functionalized PHPSs [28] were synthesized using a variety of alcohols, and successfully converted to microporous amorphous silica by oxidative crosslinking at 270°C followed by pyrolysis at 600°C in air (Route I in Fig. 3-1) [26]. However, due to the vigorous oxidation reaction of PHPSs, it was difficult to investigate the relationship between their pyrolytic behaviours and the microporous structure formation.

Herein, as continuation of our ongoing studies, alkoxy group-functionalized amorphous silica-based inorganic-organic hybrid materials were designed using room temperature oxidation

technique [8]. Then, the thermal conversion of the hybrids to microporous amorphous silica was investigated by the simultaneous thermogravimetry-mass spectrometry (TG-MS) analysis (Route II in Fig. 3-1). The relationship between the number of carbon atoms in the alkoxy group, the gaseous species formed *in-situ* during the thermal treatment and the microporosity within the final silica materials is discussed and compared with our previous results [26], in order to achieve a better understanding of the microporous structure formation in polymer-derived amorphous silica.

Perhydropolysilazane (PHPS)
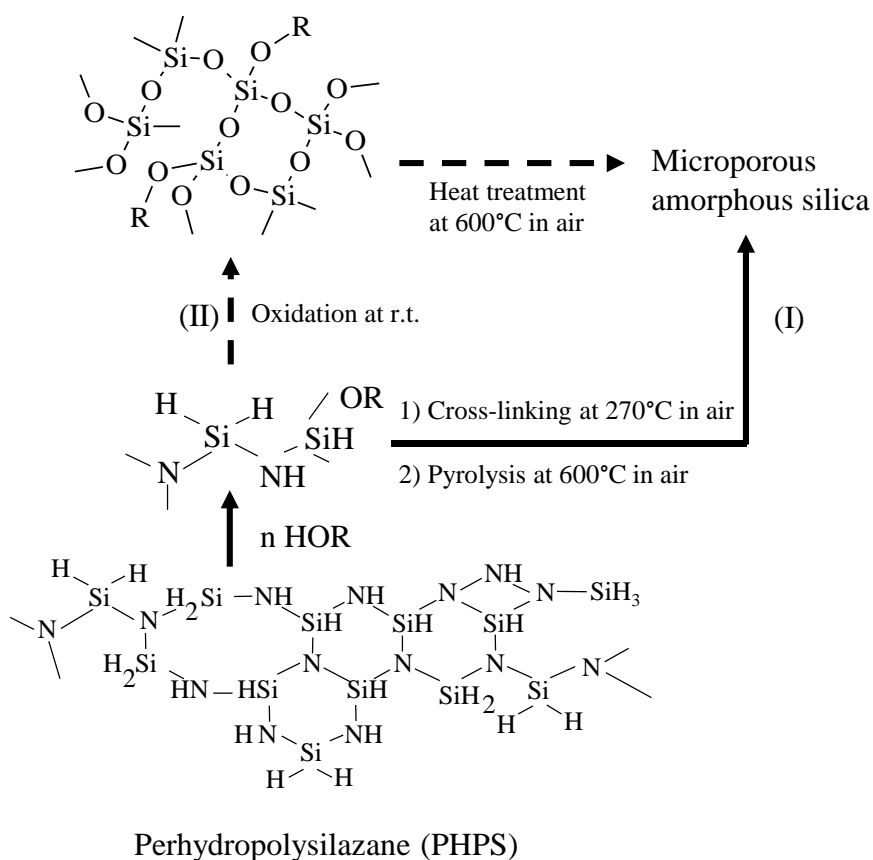
Fig. 3-1. Synthesis of microporous amorphous silica from alkoxy group-functionalized PHPS. Route I: Two-step heat treatment [26]. Route II: Oxidation step followed by heat treatment of the alkoxy group-functionalized amorphous silica intermediate.

3.2. Experimental procedures

3.2.1. Precursor synthesis

Commercially available perhydropolysilazane (PHPS, Type NN110, 20% xylene solution, AZ Electronic Materials, Japan) was used as a starting polymer. For the chemical modification of PHPS, n-pentanol (n-C_5H_{11}OH) and n-decanol (n-$C_{10}H_{21}$OH) were used. The reaction

between as-received PHPS and the alcohols was carried out under dry argon (Ar) atmosphere using Schlenk techniques [29]. PHPS (Si basis)/ROH molar ratio of 4/1 was applied for both samples, and the molar ratio of 2/1 was further investigated for the PHPS chemically modified with n-$C_{10}H_{21}OH$. In a typical procedure, the alcohol was added dropwise to a xylene solution of as-received PHPS with magnetic stirring at room temperature, followed by the addition of toluene to decrease the PHPS concentration from 20 wt% to 1 wt%. After the addition was completed, the mixture was refluxed for 1h under Ar flow and cooled down to room temperature. The xylene and toluene were removed from the reaction mixture under vacuum to give the alcohol adduct as a viscous liquid.

3.2.2. Conversion of the polymer precursor to amorphous silica-based hybrid and pyrolysis

The oxidative polymer/amorphous silica-based hybrid conversion was carried out by exposing the polymer precursor to vapour from aqueous ammonia (NH_3) according to the procedure reported by Kubo *et al.* [8] In this process, 15 mL of aqueous NH_3 was placed in a 200 mL beaker with a slightly open lid and the polymer precursor (ca. 600 mg) was suspended over the aqueous NH_3 until the silica-based hybrid formed as white powder. The resulting amorphous silica-based hybrid was ground to a fine powder using a mortar and pestle, then heat-treated in a furnace under air flow up to 600°C for a period of time of 6 h. Then the temperature was maintained at 600°C for an additional hour, and finally cooled down to room temperature to afford amorphous silica as white powders.

3.2.3. Characterization

Fourier transform infrared (FT-IR) spectra of the polymers, the polymer-derived amorphous silica-based hybrids and pyrolyzed products were recorded using KBr pellets over the range of 4000 to 400 cm^{-1} (FT/IR-4200 IF, Jasco, Japan).

The thermal behaviours up to 1000°C were studied by simultaneous thermogravimetric (TG) and mass spectroscopic (MS) analyses (Model TG/DTA6300, Hitachi High Technologies Ltd., Tokyo, Japan/Model JMS-Q1050GC, JEOL, Tokyo, Japan). The measurements were performed under flowing mixed gas of helium (He) and oxygen (O_2) (He: O_2 = 4: 1, 100 mL/min) with a heating rate of 20°C/min. To avoid the presence of dominant fragment peaks at around m/z = 32 (O_2^+) related to the presence of O_2, the m/z ratios in the range of 20 to 35 were excluded from the MS spectra for all the samples. Conventional TG analyses in air were also performed on the polymer-derived amorphous silica-based hybrids up to 1000°C at a heating rate of 100°C/h (Model TG8120, Rigaku, Tokyo, Japan), in order to examine the influence of the He and O_2 mixed gas atmosphere.

The pore size distribution for the pyrolyzed samples was determined using N_2 sorption technique with the N_2 relative pressures ranging from 0 to 0.99 (Model Belsorp Max, BEL Japan Inc., Osaka, Japan). The micropores ($r_{pore} < 2.0$ nm) and mesopores (2.0 nm $\leqq r_{pore} < 50$ nm) of the polymer-derived amorphous silica materials were characterized by the SF [30] and BJH [31] methods, respectively.

3.3. Results and discussion

3.3.1. Chemical structures identified by FT-IR spectroscopic analysis

The chemical structures of the polymeric precursors were assessed based on their FT-IR spectra. As shown in Fig. 3-2(a), as-received PHPS exhibited absorption bands at 3400 cm^{-1} (υN-H), 2150 cm^{-1} (υSi-H), 1180 cm^{-1} (δN-H) and 840-1020 cm^{-1} (δSi-N-Si) [4,26,32]. The spectra of the PHPS modified with n-C_5H_{11}OH [Fig. 3-2(b)] and that with n-$C_{10}H_{21}$OH [Fig. 3-2(c)] showed additional absorption bands at 2950-2850 cm^{-1} (υC-H), 1450 cm^{-1} (δCH$_3$), and 1090 cm^{-1} (υSi-OR) [26,32]. The intensity of the C-H absorption band remarkably increased with increasing number of carbon atom in the alcohol used for the chemical modification. By increasing Si/n-$C_{10}H_{21}$OH molar ratio from 4/1 to 2/1 [Fig. 3-2(d)], the Si-H absorption band intensity at 2150 cm^{-1} decreased remarkably while that at 1090 cm^{-1} assigned to Si-OR increased. However, a new broad absorption band assigned to υO-H [33] appeared at around 3400 cm^{-1} thus overlapping the N-H band, which suggests the existence of unreacted n-$C_{10}H_{21}$OH.

After exposure to vapours from aqueous NH_3, the absorption bands corresponding to the as-received PHPS completely disappeared, and new absorption bands appeared at 3400 (Si-OH) [33] and 1090 cm^{-1} (Si-O-Si) [33] [Fig. 3-2(a)]. In addition to these absorption bands, the spectra of the chemically modified PHPSs exhibited C-H absorption bands in the vicinity of 2950 to 2850 cm^{-1} [Figs. 3-2(b) to 3-2(d)]. These results indicate that the chemically modified PHPSs were oxidized and successfully converted to alkoxy group-functionalized amorphous silica.

The polymer derived amorphous silica-based hybrids were further heat-treated at 600°C in air. As shown in Figs. 3-2(b) to 3-2(d), the C-H absorption bands completely disappeared, and the spectra for these samples were similar to that of the 600°C heat-treated amorphous silica derived from as-received PHPS [Fig. 3-2(a)].
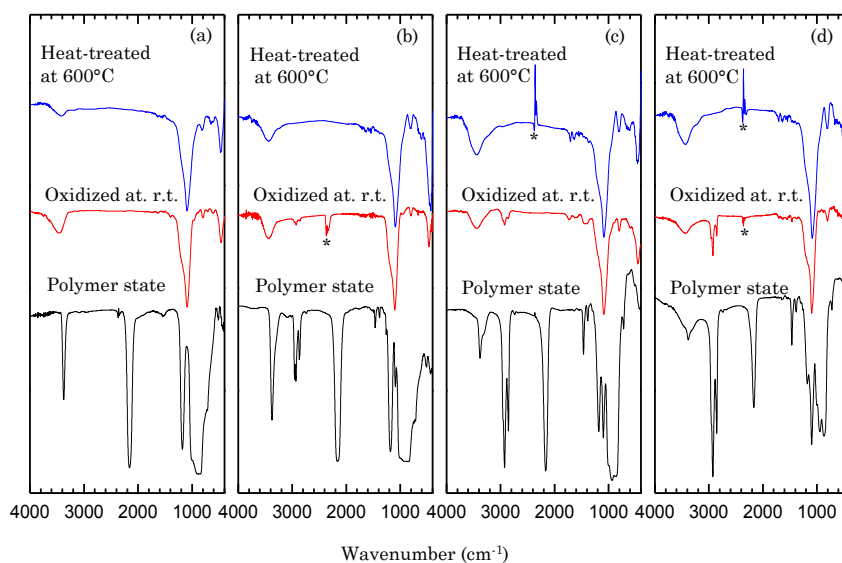
Fig. 3-2. FT-IR spectra of samples in the polymer state, after oxidation at r.t. (exposure to aqueous NH_3 vapours), and the final product after heat treatment at 600°C in air. Legend: (a) as-received PHPS, (b) $C_5H_{11}O$ group-functionalized PHPS at Si/n-$C_5H_{11}OH$ molar ratio of 4/1, (c) $C_{10}H_{21}O$ group-functionalized PHPS at Si/n-$C_{10}H_{21}OH$ molar ratio of 4/1, and (d) 2/1 (* indicating background, absorption due to CO_2).

3.3.2. Microporosity of polymer-derived amorphous silica

The textural properties of the heat-treated samples at 600°C were studied by N_2 physisorption at -196°C (77 K). The PHPS-derived amorphous silica generated a non-porous type III isotherm according to the IUPAC classification method [Fig. 3-3(a)]. The isotherm of n-$C_5H_{11}O$-modified amorphous silica exhibited a transitional type between type I and type IV without hysteresis loops. The N_2 uptake at the relative pressure lower than $P/P_o = 0.2$ is related to the micropore filling, while another slight up take above $P/P_o = 0.9$ is thought to be related to the meso- and/or macroporosity generated by agglomeration of the powdered sample. Thus, the isotherm of this sample is ascribed to type I-related microporous material [Fig. 3-3(b)]. The isotherm of n-$C_{10}H_{21}O$-modified amorphous silica also presented a similar transitional type. The N_2 uptake below $P/P_o = 0.2$ remarkably increased with increasing the carbon number in the alkoxy group from 5 to 10 [Fig. 3-3(c)], and further increase in the N_2 uptake was achieved by increasing the Si/ROH ratio from 4/1 to 2/1 [Fig. 3-3(d)].
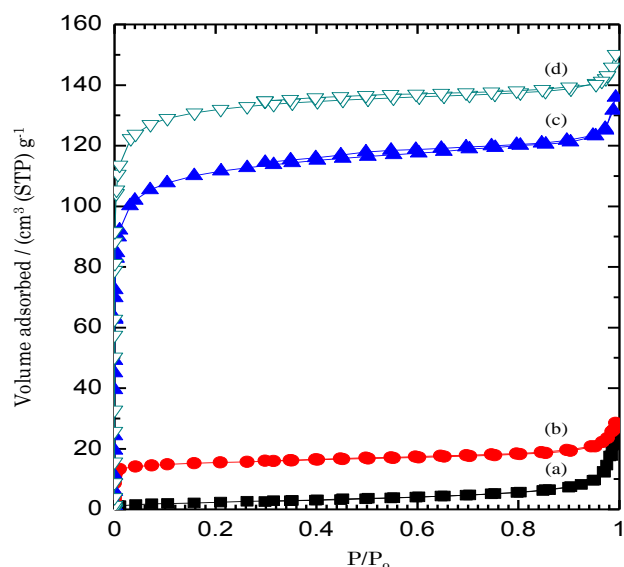
Fig. 3-3. Nitrogen sorption isotherms for samples after heat treatment at 600°C in air. Legend: (a) PHPS-derived amorphous silica. (b) $C_5H_{11}O$ group-functionalized PHPS-derived amorphous silica at Si/n-$C_5H_{11}OH$ molar ratio of 4/1, (c) $C_{10}H_{21}O$ group-functionalized PHPS-derived amorphous silica at Si/n-$C_{10}H_{21}OH$ molar ratio of 4/1, and (d) 2/1.

Figure 3-4(a) shows the pore size distribution (PSD) plots obtained for the heat-treated samples at 600°C. The micropore volumes for these samples are plotted as a function of number of carbon atoms in the alkoxy group as shown in Fig. 3-4(b). Compared with the non-porous amorphous silica, an apparent enhancement in the micropore volume was achieved by the alkoxy group-functionalization prior to the heat treatment. The micropores evaluated for the sample derived from n-$C_5H_{11}O$ group-functionalized silica were in a range of 0.43 to 1.0 nm in size. The resulting PSD plot exhibited a peak at 0.5 nm, and the micropore volume was measured to be 0.024 cm^3/g. Upon functionalization with the long alkoxy group (n-$C_{10}H_{21}O$), the PSD plot extended to approximately 1.6 nm in size, while the PSD was peaked at 0.43 nm, and the micropore volume increased to 0.173 cm^3/g. By increasing the Si/n-$C_{10}H_{21}OH$ molar ratio from 4/1 to 2/1, the PSD remained almost unchanged, while the micropore volume and specific surface area reached 0.204 cm^3/g and 387 m^2/g, respectively.
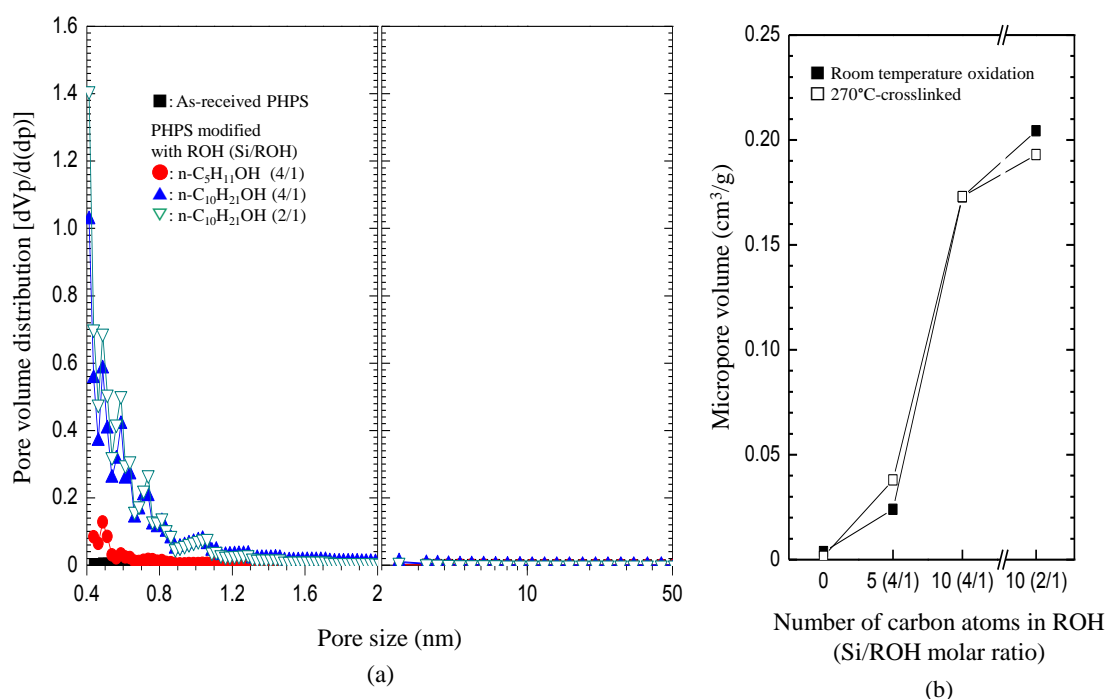
Fig. 3-4. Micro- and mesoporous structure of heat-treated samples at 600°C, evaluated by the nitrogen sorption analysis. (a) Pore size distribution. (b) Micropore volume as a function of number of carbon atoms in ROH. Between brackets are the values of (Si/ROH) molar ratios used for the chemical modification of PHPS.

The adsorption/desorption isotherms and the resulting PSD plots obtained in this study were similar to those obtained for the polymer-derived amorphous silica samples previously synthesized by the two-step heat treatment (Route I in Fig. 3-1) [26]. The variations in the micropore volumes were also compatible with those previously reported for the amorphous silica samples synthesized by the two-step heat treatment [Fig. 3-4(b)].

3.3.3. Results of TG-MS analysis

To study the pyrolytic behaviours more extensively, TG-MS analysis was performed on the polymer-derived samples after the room temperature oxidation. The results were summarized and shown in Figs. 3-5 to 3-7. The PHPS-derived amorphous silica showed a slight weight loss at 150 up to 400°C, and exhibited a weight gain of approximately 2 % at 400 up to 750°C [Fig. 3-5(a)]. The MS spectrum measured at 200°C is shown in Fig. 3-5(b). The spectrum composed of m/z ratios at 106, 91, 77, 63, 51, and 39 was identical to that reported for xylene [34,35]. Since the molecular ion (m/z =106) and the tropylium ion (m/z = 91) were detected at 150 up to 400°C [Fig. 3-5(c)], the observed weight loss is mainly due to the residual xylene, while the slight weight gain may be caused by oxidation reactions occurring at the Si-O-Si amorphous

network structural defects [36,37], as a result of the ambient temperature synthesis applied in this study.
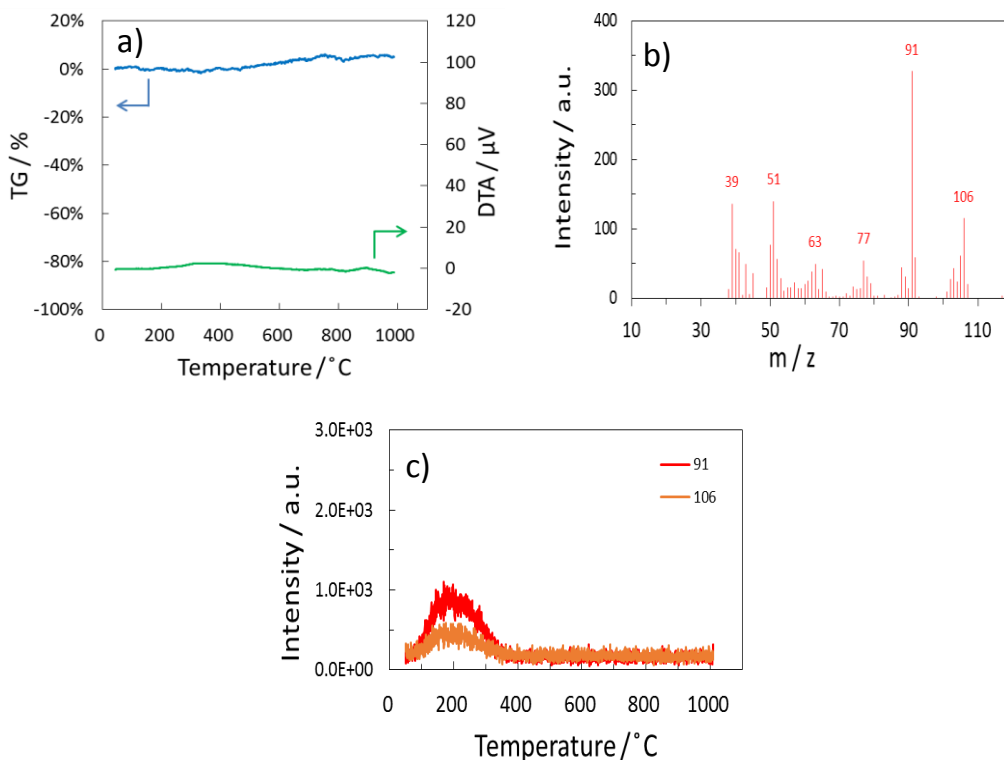

Fig. 3-5. Thermal behavior of PHPS-derived amorphous silica. a) TG-DTA, b) Monitoring of gaseous species by mass spectrometry at 200°C and (c) Continuous in-situ monitoring of gaseous species with m/z= 106 and 91 by mass spectrometry.

As shown in Fig. 3-6(a), the silica-based hybrid containing n-$C_5H_{11}O$ groups exhibited a weight loss of approximately 11 % at 150 up to 700°C, and the differential thermal analysis (DTA) resulted in the detection of a dominant exothermic peak centered at 320°C. The MS spectrum measured at 320°C is shown in Fig. 3-6(b). The m/z ratios at 57 and 43 were assigned to $C_4H_9^+$ and $C_3H_7^+$, respectively. These fragment ions could result from the α-cleavage in the n-$C_5H_{11}O$ group [34,38], while those at 70 ($C_5H_{10}^{\bullet+}$) and 55 ($C_4H_7^+$) could be derived from traces of unreacted n-$C_5H_{11}OH$ [34,39]. The smaller species, m/z ratios at 44 and 18 were assigned to CO_2^+ and H_2O^+, respectively. By monitoring the fragment ions with m/z ratios at 57 and 43, it was confirmed that the decomposition of n-$C_5H_{11}O$ group mainly occurred at 250 to 500°C [Fig. 3-6(c)]. Simultaneously, combustion of the in-situ formed hydrocarbons started at around 250°C, while the evolution of CO_2 and H_2O was detected up to approximately 650°C [Fig. 3-6(d)].

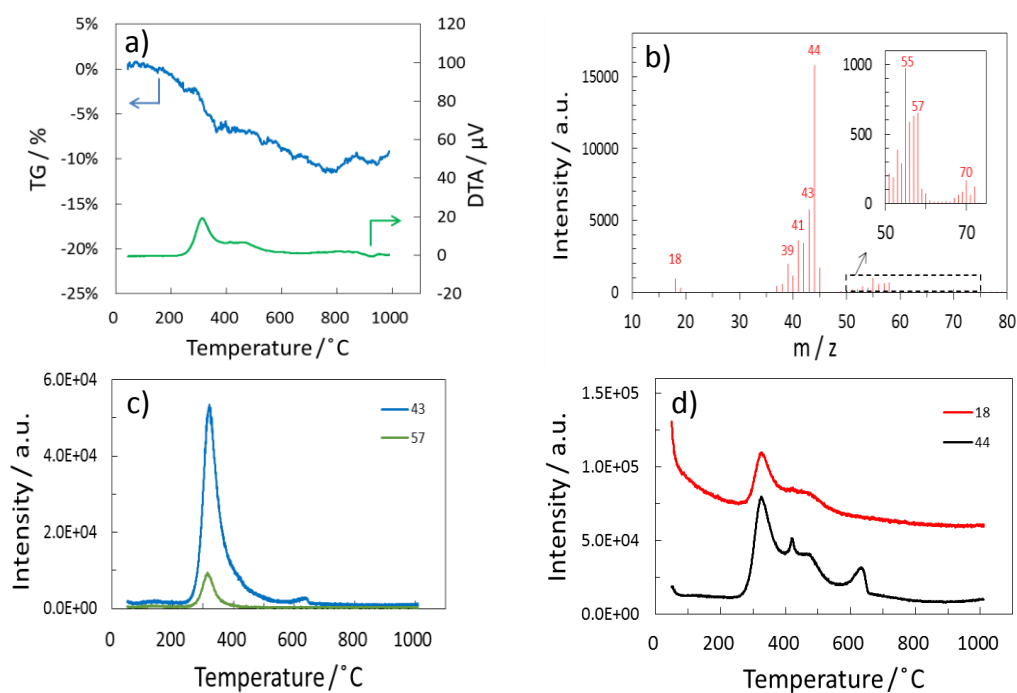Fig. 3-6. Thermal behavior of n-$C_5H_{11}O$ group-functionalized amorphous silica. a) TG-DTA, b) Monitoring of gaseous species by mass spectrometry at 200°C. Continuous in-situ of gaseous species with m/z = (c) 57 ($C_4H_9^+$), 43 ($C_3H_7^+$), and (d) 44 (CO_2^+), 18 (H_2O^+) by mass spectrometry.

With increasing number of carbon atoms in the alkoxy group from 5 to 10 as well as increasing the Si/ROH from 4/1 to 2/1, the weight loss at 150 up to 700°C increased to 55 %, and the exothermic peak became much more pronounced [Fig. 3-7(a)]. The MS spectrum measured during the weight loss exhibited sequential peaks 14 mass units apart at m/z = 85, 71, 57 and 43, which can be assigned to the fragment ions derived from hydrocarbons formed in-situ by the typical α-cleavage in the n-$C_{10}H_{21}O$ group, followed by the sequential C-C bond cleavage which releases methylene units [34,40]. However, the spectrum exhibited other peaks at m/z = 70 ($C_5H_{10}^{\bullet +}$) and 55 ($C_4H_7^+$) assigned as the fragment ions derived from n-$C_{10}H_{21}OH$ [Fig. 3-7(b)] [34,41].

The thermal decomposition and subsequent combustion behaviours for the n-$C_{10}H_{21}O$ group-functionalized silica were similar to those for the n-$C_5H_{11}O$ group-functionalized sample, while the CO_2^+ ion intensities detected at around 300°C were apparently higher than those for the n-$C_5H_{11}O$ group-functionalized sample [Figs. 3-7(c) and (d)].
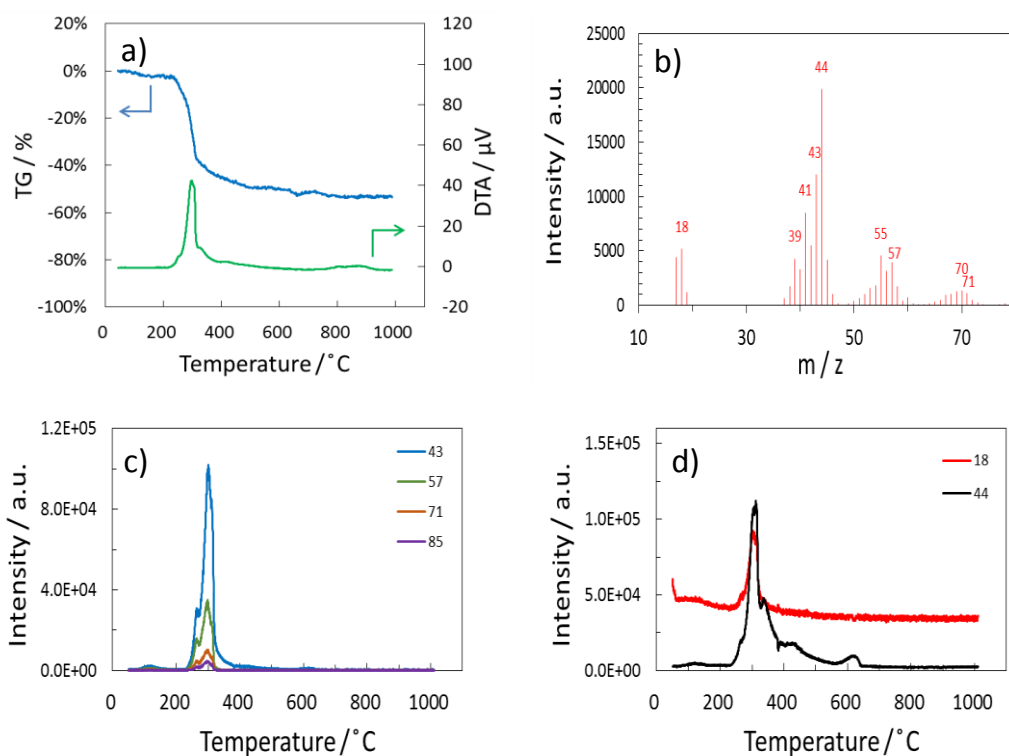
Fig. 3-7. Thermal behavior of n-$C_{10}H_{21}O$ group-functionalized amorphous silica (Si/ROH=2/1). a) TG-DTA, b) Monitoring of gaseous species by mass spectrometry at 200°C. Continuous in-situ monitoring of gaseous species with m/z = (c) 85 ($C_6H_{13}^+$), 71 ($C_5H_{11}^+$), 57 ($C_4H_9^+$), 43 ($C_3H_7^+$) and (d) 44 (CO_2^+), 18 (H_2O^+) by mass spectrometry.

3.3.4. Microporosity formations of polymer-derived amorphous silica

The intrinsic microporosity of the PHPS-derived amorphous silica heat-treated at 600°C is thought to be similar to that of the sol gel-derived amorphous silica. As for the disordered form of β-cristobalite, considered to be the generally accepted structure of glass, it is composed of 5- and 6-membered Si-O-Si rings with estimated ring size of approximately 0.3 nm [42,43]. Moreover, it has been suggested that PHPS contains 2-, 3- and 4-membered Si–N–Si ring clusters, as microporous units [5,27]. Upon oxidation at room temperature, the ring clusters are readily converted to Si-O-Si linkages, which could serve as nucleation sites for subsequent growth of micropores during the heat treatment. However, the diameters of the resulting 5- and 6-membered rings are too small for the N_2 probe molecule to access (0.364 nm) [44].Consequently, the PHPS-derived amorphous silica was characterized as non-porous.

The weight losses evaluated for amorphous silica-based hybrid containing n-$C_5H_{11}O$ group (Si/ROH=4/1) and n-$C_{10}H_{21}O$ group (Si/ROH=2/1) were compatible with those obtained by the conventional TG analysis in air (11 % and 57 %, respectively). Thus, the microporous structure

formations shown in Fig. 3-4 can be discussed based on the pyrolytic behaviours shown in Figs. 3-6 and 3-7. As mentioned above, the thermal decomposition and subsequent combustion of the alkoxy group led to the in-situ formation of gaseous species, and eventually contributed to the formation of micropores, detected using N_2 as a probe molecule. The kinetic diameters of main components of the gaseous species $C_4H_9^+$ (n-C_4H_{10}), $C_3H_7^+$ (n-C_3H_8) and CO_2 are in the range of 0.33-0.43 nm [44]. Since the micropore volume increased consistently with the number of carbon atoms in the alkoxy group as shown in Fig. 3-4(b), it is suggested that the micropore volume can be controlled by controlling the total volume of the released gaseous species formed in-situ. However, in the case of n-$C_{10}H_{21}O$ group-functionalized amorphous silica, the micropore volume did not increase linearly with the Si/ n-$C_{10}H_{21}OH$ ratio, which is due to the remaining excess of n-$C_{10}H_{21}OH$ as demonstrated by the FT-IR spectroscopy and TG-MS. The unreacted n-$C_{10}H_{21}OH$ as well as xylene which is physically trapped within the hybrid material, were released up to at 300°C. The resulting micropore units formed in-situ at the initial heat treatment step are thermodynamically unstable, and collapsed during heat treatment at 600°C. In contrast, the in-situ formation of CO_2 was found to be continuous up to approximately 650°C. Thus, among the in-situ formed small gaseous species, CO_2 could act as a particularly crucial key factor for the microporosity formation process in the amorphous silica.

In this study, microporous amorphous silica materials were successfully synthesized through the polymer-derived ceramics (PDCs) route via alkoxy group-functionalized amorphous silica-based hybrids. The amount of alkoxy group was found to play an important part in controlling the volume of micropores formed in-situ. Thus, the stoichiometric reaction between the Si-H groups in PHPS and an appropriate amount of alcohol leads to the precise control of micropore volume in the final silica material. In this respect, use of reaction catalyst such as Lewis acid would be attractive to achieve the stoichiometric reaction. It is also important to perform quantitative analysis of carbon content in the alkoxy group-functionalized amorphous silica-based hybrids. These key aspects have been given into consideration for our ongoing studies.

3.4. Conclusion

In this study, PHPS was modified with n-$C_5H_{11}OH$ and n-$C_{10}H_{21}OH$. The chemically modified PHPSs were converted to alkoxy group-functionalized amorphous silica-based inorganic-organic hybrids under room temperature oxidation, and subsequently heat-treated at 600°C in air. The results can be summarized as follows.
(1) The alkoxy group-functionalized PHPSs were successfully converted into amorphous silica-based hybrids materials by exposure to vapour from aqueous ammonia at room temperature.

(2) Alkoxy-group functionalization of silica prior to the 600°C-heat treatment in air apparently increased the micropore volume of the resulting amorphous silica, and the highest micropore volume of 0.204 cm^3/g with a specific surface area of 387 m^2/g was achieved for the sample derived from PHPS chemically modified with n-$C_{10}H_{21}OH$ at the Si/n-$C_{10}H_{21}OH$ molar ratio of 2/1.

(3) The micropores evaluated by the SF method were in the size range of 0.43 to 1.6 nm, and the resulting micropore size distribution peaked at 0.43 nm. The results of TG-MS analysis suggested that, among the in-situ formed small gaseous species including C3 and C4 hydrocarbon unit, CO_2 gas molecules, continuously released up to approximately 650°C, mainly contributed to the formation of micropores that were detected using N_2 as a probe molecule.

Table 3-1. Possible structures of compounds released from PHPS-derived silica during heat treatment in air

Compound	m/z	Chemical formula	Chemical structures	References
Water	18	H_2O		34
Carbon dioxide	44	CO_2		34
Fragments derived from xylene	106	$C_8H_{10}^{+\bullet}$ (parent ion)		34,35
	91	$C_7H_7^+$ Loss of $\bullet CH_3$ from parent ion		34,35
	77	$C_6H_5^+$ Loss of $-CH_2$ from $C_7H_7^+$		34,35
	63	$C_5H_3^+$ Loss of $-CH_2$ from $C_6H_5^+$		34,35,45
	51	$C_4H_3^+$		34,46
	39	$C_3H_3^+$ Propargyl cation		34,46

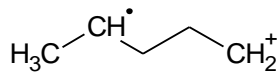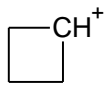Table 3-2. Possible structures of compounds released from $C_5H_{11}O$ group-functionalized PHPS during heat treatment in air
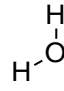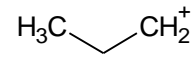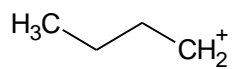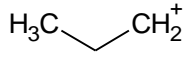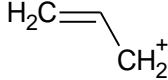
Compound	m/z	Chemical formula	Chemical structures	References
Water	18	H_2O		34
Carbon dioxide	44	CO_2		34
Fragments derived from n-pentane	43	$C_3H_7^+$ Derived from ether cleavage		34,38
	57	$C_4H_9^+$ Derived from ether cleavage		34,38
Fragments derived from n-pentanol	70	$C_5H_{10}^{+\bullet}$ Loss of H_2O		34,39
	55	$C_4H_7^+$ Loss of $\bullet CH_3$ from $C_5H_{10}^{+\bullet}$		34,39
	43	$C_3H_7^+$		34,39
	41	$C_3H_5^+$		34,39
	39	$C_3H_3^+$		34,47

50

Table 3-3. Possible structures of compounds released from $C_{10}H_{21}O$ group-functionalized PHPS during heat treatment in air

Compound	m/z	Chemical formula	Chemical structures	References
Water	18	H_2O		34
Carbon dioxide	44	CO_2	$O{=}C{=}O$	34
Fragments derived from n-decane	113	$C_8H_{17}^{+}$		34
	99	$C_7H_{15}^{+}$		34,40
	85	$C_6H_{13}^{+}$		34,40
	71	$C_5H_{11}^{+}$		34,40
	57	$C_4H_9^{+}$		34,40
	43	$C_3H_7^{+}$		34,40
Fragments derived from n-decanol	112	$C_8H_{16}^{+\bullet}$		34,41
	97	$C_7H_{13}^{+}$		34,41
	83	$C_6H_{11}^{+}$		34,41
	70	$C_5H_{10}^{+\bullet}$		34,41
	69	$C_5H_9^{+}$		34,41
	55	$C_4H_7^{+}$		34,41
	43	$C_3H_7^{+}$		34,41
	41	$C_3H_5^{+}$		34,41
	39	$C_3H_3^{+}$		34,47

References

[1] R. W. Rice, Am. Ceram. Soc. Bull., 62 (1983) 889-892.

[2] K. J. Wynne and R. W. Rice, Annu. Rev. Mater. Sci., 14 (1984) 297-334.

[3] R. Riedel, W. Dressler, Ceram. Int., 22 (1996) 233-239.

[4] D. Seyferth, C. Strohmann, N. R. Dando, A. Perrotta, J. Chem. Mater., 7 (1995) 2058-2066.

[5] E. Kroke, Y-L. Li, C. Konetschny, E. Lecomte, C. Fasel, R. Riedel, Mater. Sci. Eng., R, 26 (2000) 97-199.

[6] O. Funayama, M. Arai, Y. Tashiro, H. Aoki, T. Suzuki, K. Tamura, H. Kaya, H. Nishii, T. Isoda, J. Ceram. Soc. Japan, 98 (1990) 104-107.

[7] Y. Iwamoto, K. Sato, T. Kato, T. Inada, Y. Kubo, J. Eur. Ceram. Soc., 25 (2005) 257-264.

[8] T. Kubo, E. Tadaoka and H. Kozuka, J. Mater. Res., 19 (2004) 635–642.

[9] T. Kubo, H. Kozuka, J. Ceram. Soc. Japan, 114 (2006) 517-523.

[10] K. Miyajima, T. Eda, H. Ohta, Y. Ando, Y. Iwamoto, Ceram. Trans., 213 (2010) 87-94.

[11] C. Schitco, M. S. Bazarjani, R. Riedel, A. Gurlo, J. Mater. Chem. A, 3 (2015) 805-818.

[12] K. Kusakabe, Z. Y. Li, H. Maeda, S. Morooka, J. Membr. Sci., 103 (1995) 175-180.

[13] Z. Y. Li, K. Kusakabe, S. Morooka, J. Membr. Sci., 118 (1996) 159-168.

[14] T. Nagano, K. Sato, T. Saito, Y. Iwamoto, J. Ceram. Soc. Japan, 114 (2006) 533-538.

[15] H. Suda, H. Yamauchi, Y. Uchimaru, I. Fujiwara, K. Haraya, Desalination, 193 (2006) 252-255.

[16] R. Mourhatch, T. T. Tsotsis, M. Sahimi, J. Membr. Sci., 356 (2010) 138-146.

[17] A.Takeyama, M. Sugimoto, M. Yoshikawa, Mater. Trans., 52 (2011) 1276-1280.

[18] K.W. Völger, R. Hauser, E. Kroke, R. Riedel, Y.H. Ikuhara, Y. Iwamoto, J. Ceram. Soc. Japan, 114 (2006) 567-570.

[19] R. Hauser, S. Nahar-Borchard, R. Riedel, Y.H. Ikuhara, Y. Iwamoto, J. Ceram. Soc. Japan, 114 (2006) 524-528.

[20] R. M. Prasad, Y. Iwamoto, R. Riedel, A. Gurlo, Adv. Eng. Mater., 12 (2010) 522-528.

[21] M.S. Bazarjani, M.M. Müller, H.-J. Kleebe, Y. Jüttke, I. Voigt, M.B. Yazdi, L. Alff, R. Riedel, A. Gurlo, Appl. Mater. Interfaces, 6 (2014) 12270-12278.

[22] G. D. Soraru, Q. Liu, L. V. Interrante, T. Apple, Chem. Mater., 10 (1998) 4047-4054.

[23] Q. Liu, W. Shi, F. Babonneau, L. V. Interrante, Chem. Mater., 9 (1997) 2434–2441.

[24] L. Lee, D.S. Tsai, J. Am. Ceram. Soc., 82 (1999) 2796-2800.

[25] K. Miyajima, T. Eda, B. N. Nair, Y. Iwamoto, J. Membr. Sci., 421-422 (2012) 124-130.

[26] M. N. M. Sokri, Y. Daiko, S. Honda, Y. Iwamoto, J. Ceram. Soc. Japan, 123 (2015) 292-297.

[27] M. Weinmann, "Chapter 7 Polysilazanes", in Inorganic Materials Ed. by R. De Jaeger and

M. Gleria, Nova Science Publishers Inc., NY, USA (2007) pp. 371-413.

[28]   Y. Iwamoto, K. Kikuta, S. Hirano, J. Mater. Res., 13 (1998) 353-361.

[29]   D. F. Shiver, M.A. Drezdzon, "The manipulation of air sensitive compounds," 2nd Edition, John Wiley & Sons, Inc. (1986) pp. 30-44.

[30]   A. Saito, H.C. Foley, AIChE J., 37 (1991) 429-436.

[31]   P. Barrett, L.G. Joyner, P.H. Halenda, J. Am. Chem. Soc., 73 (1951) 373-380.

[32]   D. Seyferth, G. Wiseman, C. Prud'homme, J. Am. Ceram. Soc., 66 (1983) C-13-C-14.

[33]   R.M Silverstein, G.C. Bassler, T.C. Morrill, "Spectrometric Identification of Organic Compounds," 5th Edition, John Wiley & Sons, Inc. (1991).

[34]   S.E. Stein, "Mass Spectra" in NIST Chemistry WebBook, NIST Standard Reference Database Number 69, Eds. P.J. Linstrom and W.G. Mallard, National Institute of Standards and Technology, Gaithersburg MD, 20899, http://webbook.nist.gov, (retrieved April 2, 2015).

[35]   J.M.D. Cruz, V.V. Lozovoy, M. Dantus, J. Phys. Chem. Lett. A., 109 (2005) 8447-8450.

[36]   A.A. Chuiko, React. Kinet. Catal. Lett., 50 (1993) 1-13.

[37]   E.A. Leed, C.G. Pantano, J. Non-Cryst. Solids, 325 (2003) 48-60.

[38]   R.J. Ouellette, J.D. Rawn, "Organic Chemistry: Structure, Mechanism, and Synthesis" 1st edition, Elsevier Inc. (2014) pp. 480-482.

[39]   R.M. Smith, "Understanding Mass Spectra: A Basic Approach", 2nd edition, John Wiley & Sons, Inc. (2004) pp. 199-200.

[40]   R.A.W. Johnstone, "Mass Spectrometry for Organic Chemists" Cambridge Chemistry Texts, Cambridge University Press (1972) pp. 64-67.

[41]   J.T. Watson, O.D. Sparkman, "Introduction to Mass Spectrometry: Instrumentation, Applications, and Strategies for Data Interpretation", 4th edition, John. Wiley & Sons, Inc. (2013) pp. 368-376.

[42]   S.T. Oyama, D. Lee, P. Hacarlioglu, R.F. Saraf, J. Membr. Sci., 244, (2004) 45-53.

[43]   P. Hacarlioglu, D. Lee, G.V. Gibbs, S.T. Oyama, J. Membr. Sci., 313 (2008) 277-283.

[44]   D.W. Breck, "Zeolite Molecular Sieves", John Wiley & Sons, New York (1974), p.636.

[45]   B. Yang, C. Huang, L. Wei, J. Wang, L. Sheng, Y. Zhang, F. Qi, W. Zheng, W. Li, Chem. Phys. Lett., 424 (2006) 321-326.

[46]   M. Frenklach, H. Wang, "Aromatics Growth beyond the First Ring and the Nucleation of Soot Particles". Preprints of the 202nd ACS National Meeting, 36 (1991) pp. 1509.

[47]   A. Cameron, J. Leszczynski, M.C. Zerner, B. Weiner, J. Phys. Chem, 93 (1989) 139-144.

Chapter 4. Hydrophobicity of amorphous silica-based inorganic-organic hybrid materials derived from perhydropolysilazane chemically modified with alcohols

4.1. Introduction

Recently, photocatalytic water splitting has received considerable attention because of its significant potential for allowing low-cost, environmental-friendly hydrogen (H_2) production [1]. Due to the co-production of gaseous H_2 and oxygen (O_2), this method requires the use of efficient gas separation technology to generate pure H_2. Membrane separation is one of the most attractive H_2 gas purification technologies, and amorphous silica membranes with micropores approximately 0.3 nm in diameter show promise with regard to H_2 separation [2]. However, it has been reported that H_2 flux through microporous amorphous silica membranes decreases with time in humid environments [3,4]. The hydrophilic nature of the amorphous silica resulting from the presence of surface silanol groups (Si-OH) leads to the blockage of micropores by adsorbed water at low temperatures [3]. In addition, at high temperatures such as are encountered during the methane steam reforming reaction, the H_2 permselectivity is decreased by the degradation of the silica network structures. To date, these issues have limited the practical applications of such membranes [5,6]. Thus, in order to enhance the hydrostability of amorphous silica in humid environments, surface modification of silica has been widely studied, including the modification of Si-H groups with organic moieties to Si-R, where R is an alkyl group [7,8]. The presence of organic groups has a significant effect in terms of increasing the hydrophobicity of the silica [7,9].

Perhydropolysilazane (PHPS) has been studied as a useful polymer precursor for the synthesis of pure silica, as it is readily oxidized to yield pure silica with a high ceramic yield, either by pyrolysis in air [10] or by exposure to vapour from aqueous ammonia at room temperature [11,12]. Iwamoto *et al*. [10] reported an approach in controlling the micro- and meso-porous structure formation using methyl-substituted polysilazane precursor, in which the methyl group acted as a sacrificial template during polymer to ceramic conversion by heat treatment in air, generating the micro- and mesoporous structures.
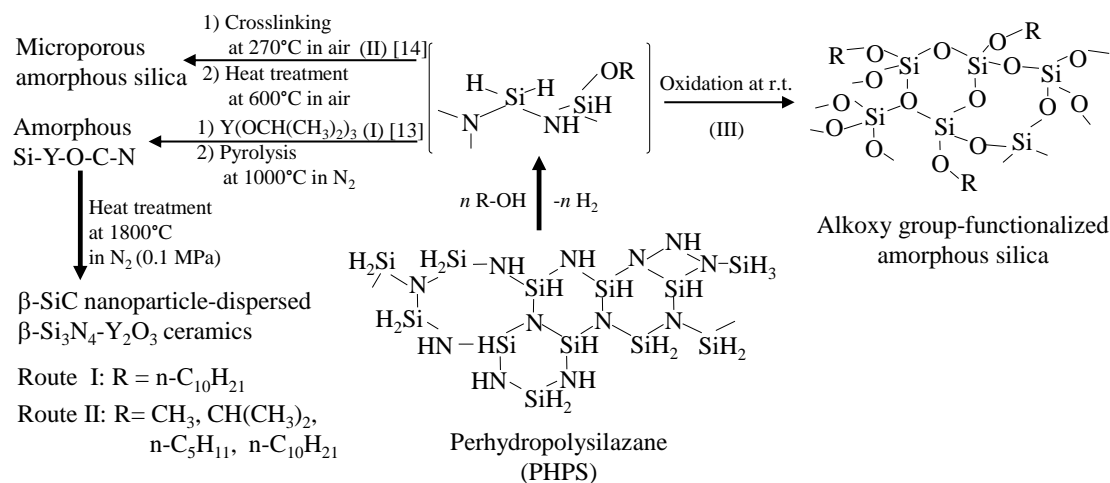
Microporous amorphous silica ← 1) Crosslinking at 270°C in air (II) [14] / 2) Heat treatment at 600°C in air

Amorphous Si-Y-O-C-N ← 1) Y(OCH(CH₃)₂)₃ (I) [13] / 2) Pyrolysis at 1000°C in N₂

1) Crosslinking at 270°C in air (II) [14]
2) Heat treatment at 600°C in air
1) Y(OCH(CH₃)₂)₃ (I) [13]
2) Pyrolysis at 1000°C in N₂

Heat treatment at 1800°C in N₂ (0.1 MPa)

β-SiC nanoparticle-dispersed β-Si₃N₄-Y₂O₃ ceramics

Route I: R = n-C₁₀H₂₁
Route II: R= CH₃, CH(CH₃)₂, n-C₅H₁₁, n-C₁₀H₂₁

(III)   Oxidation at r.t.

n R-OH -n H₂

Perhydropolysilazane (PHPS)

Alkoxy group-functionalized amorphous silica

Fig. 4-1. Synthetic route for alkoxy group-functionalized amorphous silica-based inorganic organic hybrids investigated in this study (Route III) in comparison with those for β-SiC nanoparticle-dispersed β-Si₃N₄-Y₂O₃ ceramics (Route I) [13] and microporous amorphous silica (Route II) [14] via alkoxy group-functionalized PHPSs discussed in Chapter 3.

In our recent study, alkoxy group-functionalized PHPS was synthesized as an intermediate compound to synthesize a single source precursor for Si-Y-O-C-N multicomponent ceramic system [13]: PHPS was reacted with n-decanol (n-C₁₀H₂₁OH) to afford n-C₁₀H₂₁O group functionalized PHPS. This polymer was further modified with yttrium tri-methoxide [Y(OCH₃)₃]. The resulting single source precursor was successfully converted to β-SiC nanoparticle-dispersed β-Si₃N₄-Y₂O₃ pseudo binary ceramics by pyrolysis at 1000°C followed by heat treatment at 1800°C in N₂ (Route I in Fig. 4-1). Then, as discussed in Chapter 2, alkoxy group-functionalized PHPSs were synthesized using various alcohols (ROH, R=CH₃, CH(CH₃)₂, n-C₅H₁₁ and n-C₁₀H₂₁) as chemical modifiers and successfully converted to microporous amorphous silica by oxidative crosslinking at 270°C followed by heat treatment at 600°C in air. [14] (Route II in Fig. 4-1). Moreover, as discussed in Chapter 3, alkoxy group-functionalized amorphous silica-based inorganic-organic hybrid materials were successfully isolated as intermediates for the polymer-derived microporous amorphous silica after chemical modification of PHPS with alcohols and subsequent room temperature oxidation in air [15].

As mentioned in Chapter 1, the introduction of alkyl groups to amorphous silica surfaces is effective to enhance the hydrostability of silica by making it hydrophobic. In addition to the introduction of alkyl groups to amorphous silica surfaces, the conversion of polar hydroxy (OH) groups to nonpolar alkoxy (OR) groups on silica surfaces can be expected to improve stability under humid conditions by enhancing the hydrophobicity of amorphous silica. In the present study, alkoxy group-functionalized amorphous silica-based inorganic-organic hybrid materials

were designed and synthesized from PHPS chemically modified with alcohols and alcohol derivatives using the room temperature oxidation technique (Route III in Fig. 4-1).

The water vapour sorption behaviour related to the different alkoxy groups of the hybrid materials was subsequently assessed and discussed with the aim of developing a stable hydrogen gas separation membrane that functions under humid photocatalytic water splitting conditions at room temperature.

4.2. Experimental procedures

4.2.1. Precursor Synthesis

Commercially available perhydropolysilazane (PHPS, Type NN110, 20% xylene solution, AZ Electronic Materials, Japan) was used as the starting polymer. Various alcohols, including methanol (CH_3OH), n-propanol (C_3H_7OH), n-pentanol ($C_5H_{11}OH$), n-decanol ($C_{10}H_{21}OH$), 2-methoxyethanol ($CH_3OC_2H_4OH$) and 2-ethoxyethanol ($C_2H_5OC_2H_4OH$), were used for the chemical modification of the PHPS. The reaction between the as-received PHPS and each alcohol was carried out under a dry argon (Ar) atmosphere using Schlenk techniques [16]. A PHPS (Si basis)/ROH molar ratio of 3:1 was applied in all cases.

In each synthesis, the alcohol was added dropwise to a xylene solution of as-received PHPS with magnetic stirring at room temperature, followed by the addition of toluene to decrease the PHPS concentration from 20 wt% to 1 wt%. After the addition was complete, the mixture was refluxed for 1 h under an Ar flow and cooled to room temperature. The xylene and toluene were removed from the reaction mixture under vacuum to give the alcohol adduct as a viscous liquid.

4.2.2. Conversion of the polymer precursor to amorphous silica-based hybrid

The oxidative polymer/silica-based hybrid conversion was carried out by exposing the polymer precursor sample to vapour from aqueous ammonia (NH_3) according to the procedure reported by Kubo *et al*. [11]. In this process, 15 ml of aqueous NH_3 was placed in a 200 mL beaker with a slightly open lid and the polymer precursor sample was suspended over the aqueous NH_3 until a white solid was formed. The resulting white solid was then ground to a fine powder using a mortar and pestle.

4.2.3. Characterization

Fourier transform infrared (FT-IR) spectra of the polymers and the polymer-derived amorphous silica-based hybrids were recorded using KBr pellets over the range of 4000 to 400 cm^{-1} (FT/IR-4200 IF, Jasco, Japan). The density of Si-OH groups in each polymer-derived amorphous silica-based hybrid was determined from the relative ratio of the FT-IR band

absorption intensities at 3400 and 1090 cm^{-1}: $I_{Si\text{-}OH}/I_{Si\text{-}O\text{-}Si}$. ^{1}H nuclear magnetic resonance (NMR) spectra were acquired for the original alcohols, as-received PHPS and chemically modified PHPSs in CDCl$_3$ solution at room temperature (AV400N, Bruker, USA).

The pore size distribution for the powder samples was determined using a N$_2$ sorption technique with the relative pressure of the N$_2$ gas ranging from 0 to 0.99 (Belsorp Max, BEL Japan Inc., Osaka, Japan). The micropores ($r_{pore} < 2.0$ nm) and mesopores (2.0 nm $\leqq r_{pore} < 50$ nm) of the polymer-derived amorphous silica-based hybrid samples were characterized by the SF [17] and BJH [18] methods, respectively. The hydrophobicity of each polymer-derived hybrid was assessed by isothermal water vapour sorption at 25°C (298 K) using adsorption and desorption isotherms (BEL Aqua, BEL Japan Inc., Osaka, Japan). In addition, the N$_2$ and water vapour sorption of commercially available mesoporous silica (TMPS, Taiyo Kagaku, Tokyo, Japan) were measured as a reference.

To estimate the chain length of the alkoxy group (OR) introduced to silica, molecular structure calculations based on the Hartree-Fock theory (HF) were performed. Basis set of 6-31*G(d) was used for the calculations. The estimated chain length for each OR group is shown in Table 4-1, and used for discussion on hydrophobicity of alkoxy group-functionalized amorphous silica-based hybrids investigated in this study.

Table 4-1. Properties of alkoxy group-functionalized amorphous silica-based hybrids synthesized through polymer precursor route.

Name	Alkoxy group (OR)		BET surface area (m^2/g)	Mean mesopore size (nm)
	R	Length of OR (nm)		
C$_0$	None	-	121.6	16.3
C$_1$	CH$_3$	0.143	156.2	25
C$_3$	n-C$_3$H$_7$	0.374	222.1	17.5
C$_5$	n-C$_5$H$_{11}$	0.625	200.4	11.5
C$_{10}$	n-C$_{10}$H$_{21}$	1.248	456.5	3.3
C$_{1O1}$	CH$_3$OC$_2$H$_4$	0.476	336.4	49.7
C$_{1O2}$	C$_2$H$_5$OC$_2$H$_4$	0.607	288.3	46
TMPS	None	-	893.4	3.7

4.3. Results and discussion

4.3.1. Chemical structures of precursors

The chemical structures of the polymeric precursors were assessed based on their FT-IR

spectra. As shown in Fig. 4-2A(a), the as-received PHPS exhibited absorption bands at 3400 (υN-H), 2150 (υSi-H), 1180 (δN-H) and 840-1020 cm^{-1} (δSi-N-Si) [19,20]. The spectra of the PHPS following modification with the alcohols [Figs. 4-2A(b)-(g)] presented additional absorption bands at 2950-2850 (υC-H), 1450 (δCH$_3$) and 1090 cm^{-1} (υSi-OR) [21]. When using R′OC$_2$H$_4$OH (R' = CH$_3$, C$_2$H$_5$) for the chemical modification of PHPS, the absorption band at 1180 cm^{-1} (δN-H) could no longer be observed in the post reaction product, while the absorption band at 3400 cm^{-1} became broader in comparison with that of the as-received PHPS, suggesting the formation of Si-OH. These samples were found to be highly reactive toward ambient moisture and were readily oxidized during the sample transfer and loading steps associated with the FT-IR spectroscopic analysis.
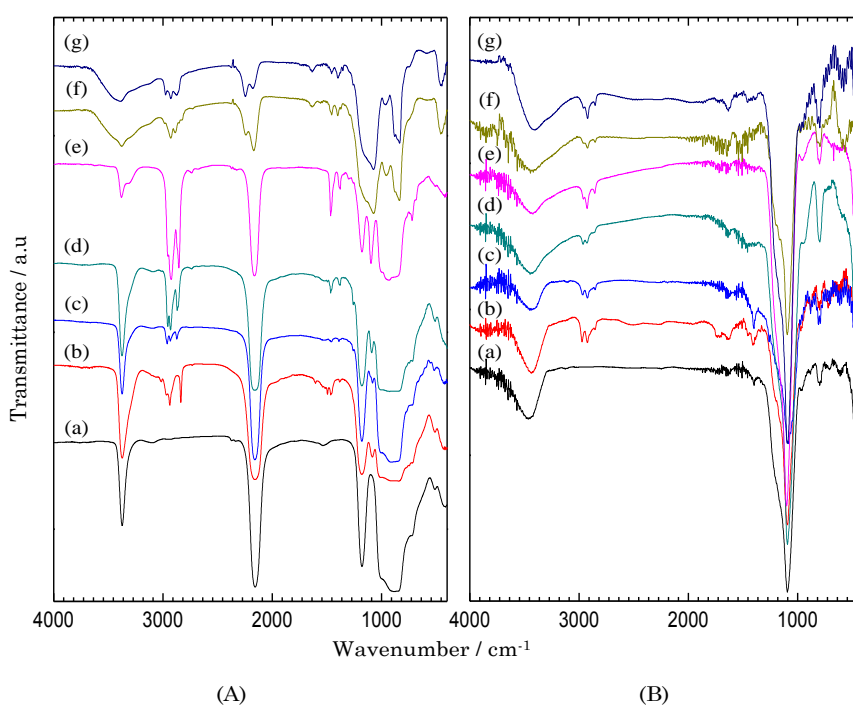
Fig. 4-2. IR spectra of samples (A) in the polymer state and (B) after exposure to aqueous NH$_3$ vapour. Legend: (a) PHPS and PHPS modified with (b) CH$_3$OH, (c) n-C$_3$H$_7$OH, (d) n-C$_5$H$_{11}$OH, (e) n-C$_{10}$H$_{21}$OH, (f) CH$_3$OC$_2$H$_4$OH and (g) C$_2$H$_5$OC$_2$H$_4$OH.

The reaction between PHPS and alcohols was further studied by ^{1}H-NMR spectroscopic analysis. As typical results, the ^{1}H-NMR spectrum of as-received PHPS is shown in Fig. 4-3(a), and those of as-received n-C$_3$H$_7$OH and PHPS chemically modified with n-C$_3$H$_7$OH are presented in Fig. 4-3(b). The as-received PHPS generated broad peaks at 5.2-4.5, 4.3 and 1.8-1.0 ppm, assigned to SiH/SiH$_2$, SiH$_3$ and NH, respectively [11,22]. The sharp peaks observed around 2.2 ppm are due to residual toluene. The ^{1}H-NMR spectrum of the PHPS

modified with n-C$_3$H$_7$OH mainly consists of peaks resulting from the PHPS and the n-C$_3$H$_7$O groups. However, the peak resulting from the n-C$_3$H$_7$OH hydroxyl proton (H$_D$) at 3.3 ppm has disappeared while the peaks due to the n-C$_3$H$_7$O group are broader in comparison with those in the spectrum of n-C$_3$H$_7$OH, indicating the formation of the polymer network. Moreover, a new peak appeared at 4.69 ppm thus overlapped the broad SiH/SiH$_2$ peak, indicating the formation of HSiON$_2$ groups [13]. Similar results have been previously reported for PHPS chemically modified with n-C$_{10}$H$_{21}$OH, and thus these data suggest that the alcohols investigated in this study primarily reacted with the H$_2$SiN$_2$ groups of the PHPS to form RO-SiHN$_2$ moieties [13, 14].
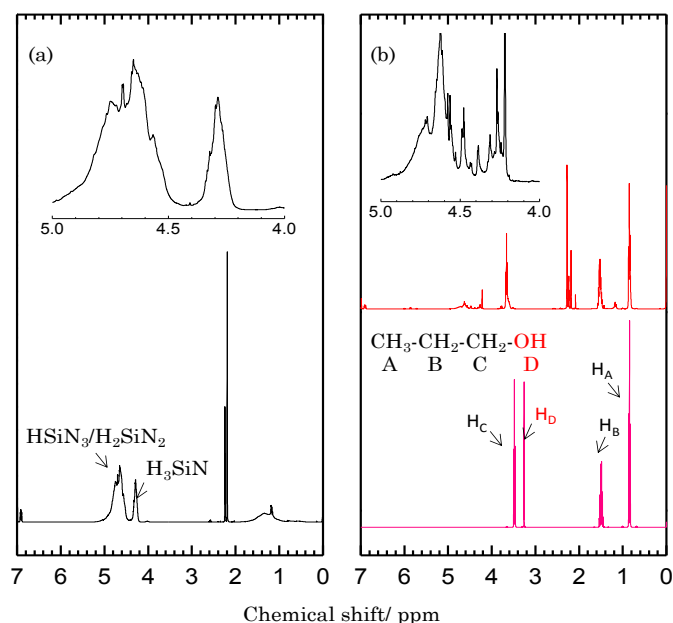
Fig. 4-3. ^{1}H-NMR spectra of (a) as-received PHPS and (b) n-C$_3$H$_7$OH and PHPS modified with n-C$_3$H$_7$OH.

After exposure to vapour from aqueous NH$_3$, the absorption bands corresponding to the as-received PHPS completely disappeared and new absorption bands were observed at 3400 (Si-OH) and 1090 cm^{-1} (Si-O-Si) [21] [Fig. 4-2B(a)].The spectra of the chemically modified PHPSs exhibited C-H absorption bands in the vicinity of 2950 to 2850 cm^{-1} [Figs. 4-2B(b)-(g)]. These results indicate that as-received PHPS and the chemically modified PHPSs were successfully converted to amorphous silica, and alkoxy group-functionalized inorganic-organic hybrid silica materials, respectively (Route III in Fig. 4-1).

4.3.2. Porous structures of the hybrid powders

The textural properties of the PHPS-derived amorphous silica-based hybrids were studied by N_2 physisorption at -196°C (77 K). The adsorption/desorption isotherms are presented in Fig. 4-4 and the sample names are listed in Table 4-1. The commercial silica sample (TMPS) generated a typical type IV mesoporous isotherm according to the IUPAC classification method [22,23], as recognized by the appearance of a hysteresis loop, the defining feature associated with the occurrence of mesopore condensation. Although the maximum value of V_a varied from approximately 260 to 790 cm^3 (STP) g^{-1}, the PHPS-derived amorphous silica (C_0) and the silica-based hybrid samples also exhibited similar type IV isotherms with hysteresis loops.
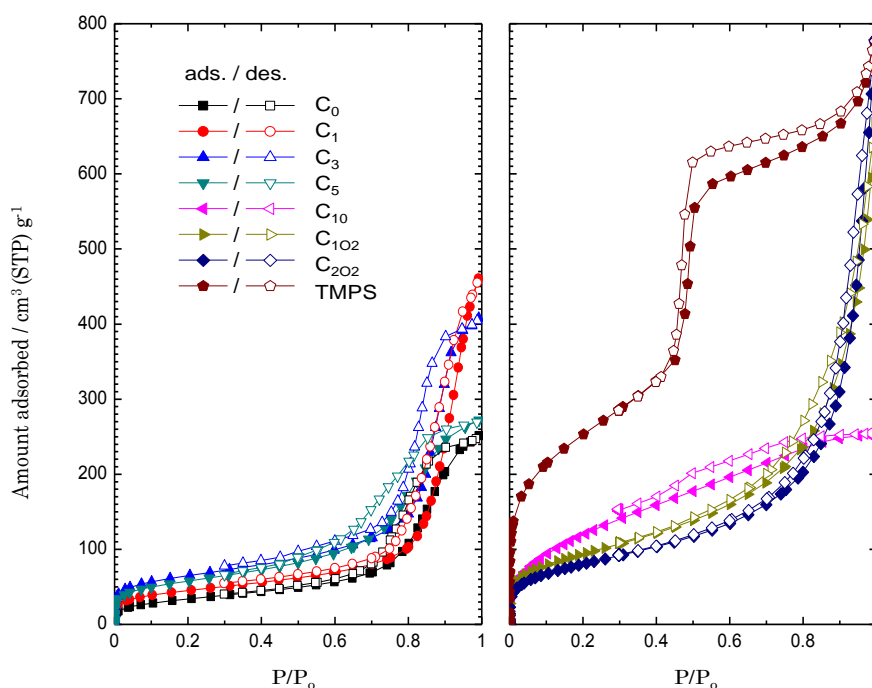
Fig. 4-4. Nitrogen sorption isotherms for amorphous silica-based samples.

Fig. 4-5 shows the pore size distribution (PSD) plots obtained for all the samples. The PSD curves for the micropores ($r_{pore} < 2.0$ nm) and those for the mesopores (2.0 nm $\leqq r_{pore} < 50$ nm) were determined using the SF [17] and BJH [18] methods, respectively. The PSD curve for TMPS is also included separately in this figure. TMPS shows a high mesopore volume with a narrow PSD peak centred at 3.7 nm. The PHPS-derived silica-based hybrid samples exhibit a small amount of micropores less than 0.9 nm in size, along with mesopores having a relatively wide PSD. The PSD plots for C_1, C_{1O2} and C_{2O2} are especially wide and extend to above 50 nm in size, thus entering the macropore size range.
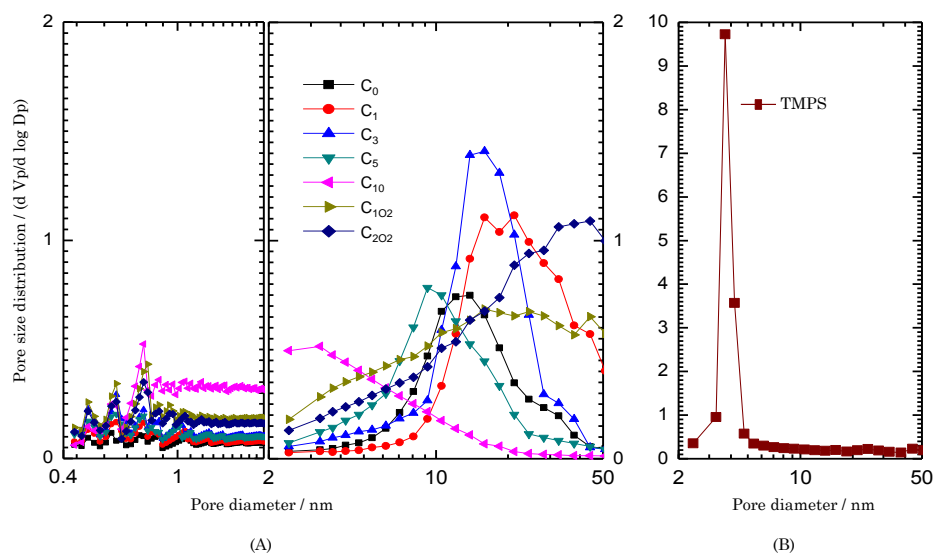
Fig. 4-5. Pore size distributions for (A) amorphous silica-based samples and (B) TMPS.

As shown in Table 4-1, compared with TMPS (893.4 m^2/g), C_0 exhibited a much lower SSA value of 121.6 m^2/g and, with the exception of the methoxyethyl- (C_{1O2}) and ethoxyethyl-group functionalized (C_{2O2}) samples, there was a tendency for SSA to increase with increasing number of carbon atoms in the alkoxy group, while the mean mesopore size decreased with increasing number of carbon atoms.

4.3.3. Water vapour sorption properties of hybrids

The hydrophilic/hydrophobic characteristics of the silica-based hybrid samples were assessed by water vapour sorption at 25°C (298 K). The adsorption/desorption isotherms are shown in Fig. 4-6, in which the SSA values from Table 4-1 were used to calculate the number of H_2O molecules adsorbed per square nanometre of the sample surface area (normalized by the SSA).

TMPS presents a major increase in H_2O sorption at higher humidity, with $P/P_o > 0.6$, and the associated isotherms can be classified as type V, signifying weak interactions between adsorbent and adsorbate [23,24]. Since H_2O molecules are highly polar, at higher humidity the mesopores could be filled due to the strong interactions between newly attached H_2O molecules and H_2O molecules already adsorbed at lower humidity, leading to the condensation that generated a significant type H4 hysteresis loop [23,24]. The normalized maximal H_2O sorption for the TMPS was 34 mol nm^{-2}. This value is compatible with that reported for the as-synthesized mesoporous silica FSM-16 (approximately 26 mol nm^{-2}) [25].
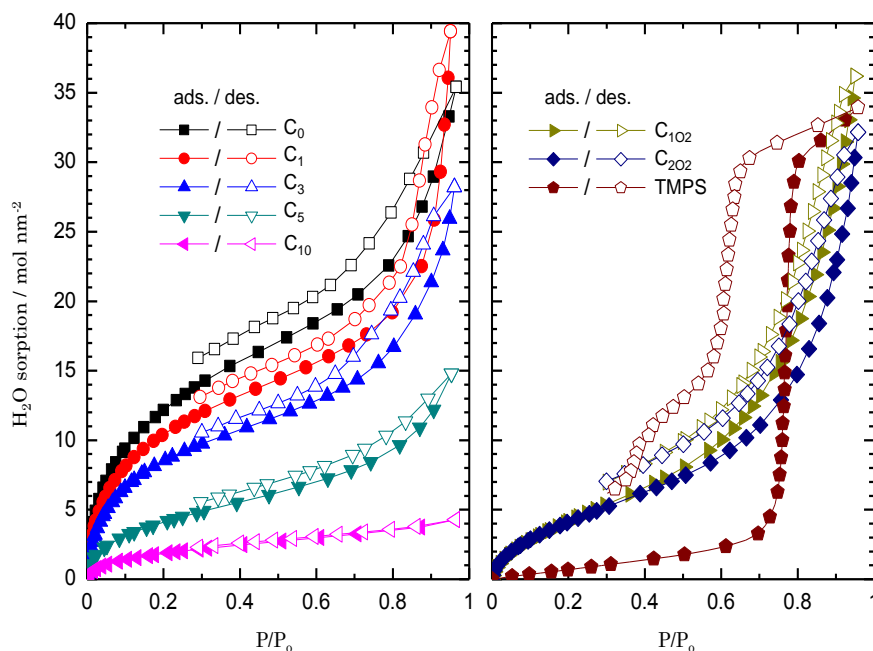
Fig. 4-6. Water vapour sorption isotherms for amorphous silica-based samples. The sorption values were calculated using the SSA data in Table 4-1.

The PHPS-derived amorphous silica (C_0), and amorphous silica-based hybrids generated type IV isotherms with type H3 loops, normally observed in the case of solids having cylindrical and spherical pores [23,24]. The normalized maximal H_2O sorption values for C_0, C_1, C_{1O2} and C_{2O2} were in the range of 32 to 39.5 mol nm^{-2}. Compared with these samples, C_3, C_5 and C_{10} showed lower values and, among the three samples, the values decreased with increasing number of carbon atoms. As a result, the normalized maximal H_2O sorption for C_{10} was as low as 4 mol nm^{-2}.

To study the hydrophilic/hydrophobic characteristics in more detail, H_2O adsorption was analyzed by dividing the data into two P/P_o regions: a lower region at and below $P/P_o = 0.6$ and a higher one above $P/P_o = 0.6$, as shown in Figs. 4-7 and 4-8, respectively. At lower humidity (Fig. 4-7), H_2O adsorption increased with increasing humidity (P/P_o) and, except for those samples having $R'OC_2H_4O$ [$R' = CH_3$ (C_{1O2}) and/or C_2H_5 (C_{2O2})] groups, the H_2O adsorption decreased with increasing number of carbon atoms. Compared with the PHPS-derived samples, TMPS showed higher hydrophobicity and the normalized H_2O adsorption at $P/P_o = 0.6$ for this sample was 2.2 mol nm^{-2}, a value comparable to that obtained for C_{10} (approximately 3 mol nm^{-2}).
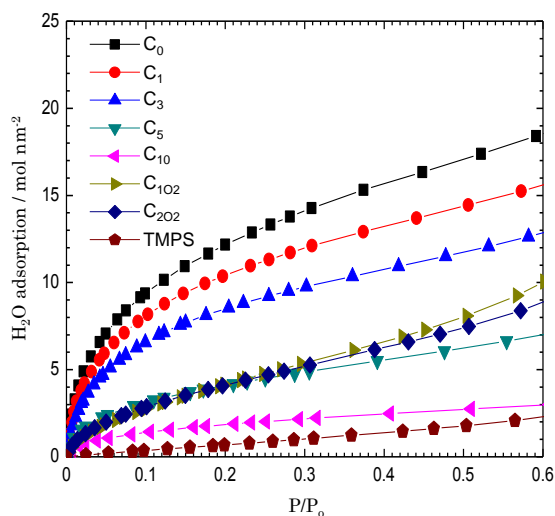
Fig. 4-7. Water vapour adsorption for amorphous silica-based samples at $P/P_o \leqq 0.6$. The adsorption values were calculated using the SSA data in Table 4-1.

At higher humidity in the vicinity of $P/P_o = 0.6$ (Fig. 4-8), the H_2O adsorption for TMPS showed a rapid increase at approximately $P/P_o = 0.75$, reaching 30 mol nm^{-2} at $P/P_o = 0.8$, which was the highest among the samples investigated in this study. Above $P/P_o = 0.8$, with the exception of C_5 and C_{10}, the PHPS-derived samples also showed a rapid increase in H_2O adsorption. At $P/P_o = 0.95$, H_2O adsorption for these samples was in the range of 28 to 39.5 mol nm^{-2}. In contrast, C_5 and C_{10} exhibited superior hydrophobicity. In particular, H_2O adsorption for C_{10} was approximately 4 mol nm^{-2} and was almost constant even at high humidity.
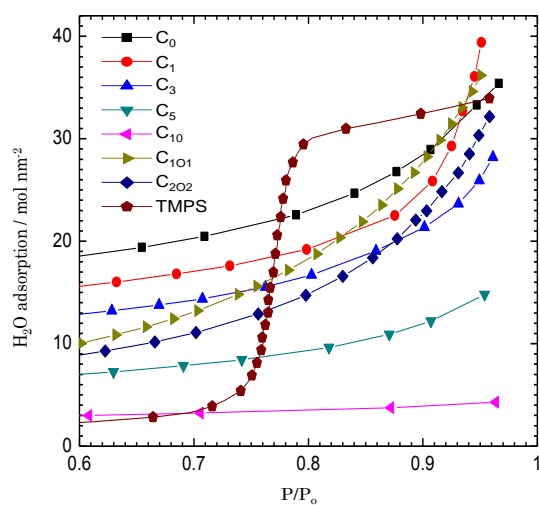

Fig. 4-8. Water vapour adsorption for amorphous silica-based samples at $P/P_o > 0.6$. The adsorption values were calculated using the SSA data in Table 4-1.

Burneau *et al.* [26] found that the initial hydration layer on porous silica is non-uniform and involves essentially unconnected H_2O molecules, and that the extent of H_2O adsorption in this layer corresponds roughly to the number of hydroxyl groups [26]. To study the formation of the first hydration layer on the samples investigated in this study, the relationship between the chain length of the alkoxy (OR) group and H_2O adsorption at $P/P_o = 0.6$ was plotted, as shown in Fig. 4-9(a). During adsorption at lower humidity, there was an apparent tendency for H_2O adsorption to decrease with increasing chain length of the OR group. However, it was not a simple linear relationship. Then, the density of hydroxyl groups and H_2O adsorption at $P/P_o = 0.6$ was plotted [Fig. 4-9(b)] and analysed. The density of Si-OH group in the samples was evaluated from the ratio of the FT-IR band intensities: I_{Si-OH} at 3400 cm^{-1}/$I_{Si-O-Si}$ at 1090 cm^{-1}. Except for C_{1O2} and C_{2O2}, the Si-OH group density for each PHPS-derived sample decreased with increasing number of carbon atoms, *i.e.* the chain length of OR group, and the H_2O adsorption linearly decreased with decreasing OH density. The H_2O adsorption was thus found to be largely governed by the density of OH groups. As shown in Fig. 4-9(a), the chain lengths estimated for C_{1O2} and C_{2O2} are compatible with that of C_5, while, in spite of having a higher OH density, both C_{1O2} and C_{2O2} exhibited lower H_2O adsorption. These results suggest that the ether groups $R'OC_2H_4$ ($R' = CH_3$ and/or C_2H_5) are effective at suppressing H_2O adsorption to some extent.
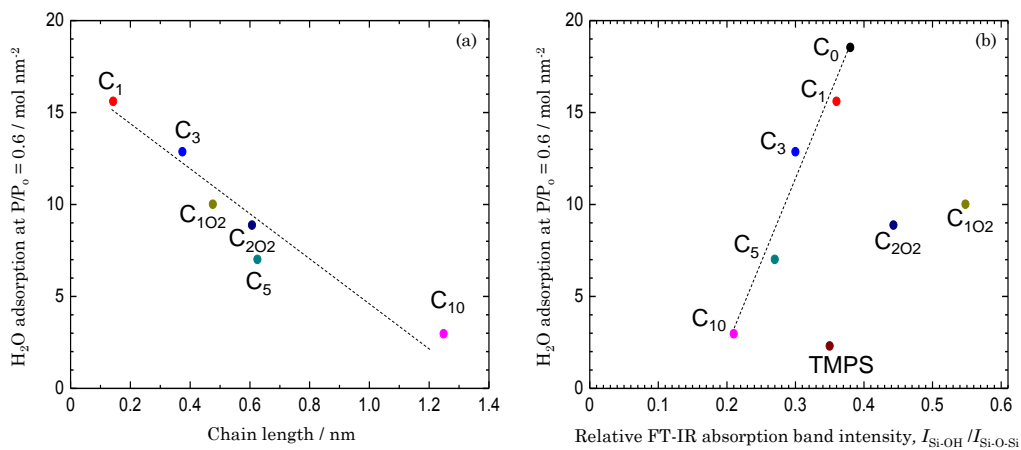

Fig. 4-9. Water vapour adsorption at $P/P_o = 0.6$ as a function of (a) chain length of alkoxy group (OR), and (b) hydroxyl group density. The adsorption values were calculated using the SSA data in Table 4-1.

Compared with TMPS, the PHPS-derived samples investigated in this study were hydrophilic, which may have been due to structural defects in the Si-O-Si amorphous network [27,28] resulting from the ambient temperature synthesis applied.

To recognize the intrinsic hydrophilic/hydrophobic properties at higher humidity, effects of the following two parameters, the chain length of OR group and the density of OH groups on the H_2O adsorption at $P/P_o = 0.95$ were examined. Since the amorphous silica-based samples investigated in this study were mesoporous (Fig. 4-5), it should be taken into account that capillary condensation occurs at elevated humidity ($P/P_o > 0.6$). According to Lodewyckx *et al*. [29], at higher humidity the micropore system is completely filled with H_2O, and additional H_2O is adsorbed at the external surfaces or, as in the present study, the mesopores. Thus, the relative amount of water within the mesopores was used as a basis for evaluation by dividing the total volume of water adsorption at $P/P_o = 0.95$ by the mesopore volume [$V_{mesopore}(N_2)$] determined from N_2 sorption isotherms. As shown in Fig. 4-10(a), except for C_{1O2} and $C_{2O2,}$ the hybrids having an aliphatic carbon substituent (C_1, C_3, C_5 and C_{10}) showed the H_2O adsorption trend similar to that observed at lower humidity, and as can be seen from Fig. 4-10(b), the H_2O adsorption of the PHPS-derived samples increased linearly with the OH density. However, H_2O adsorption for these samples was apparently lower than that for TMPS. Then, the effect of mesopore size on the capillary condensation was further examined. As shown in Fig. 4-5, TMPS represented mesoporous silica with a sharp PSD peak at 3.7 nm, possibly leading to a kind of confinement effect that enhanced the capillary condensation governed by the strong interactions between H_2O molecules and H_2O molecules bonded to Si-OH groups at lower humidity.
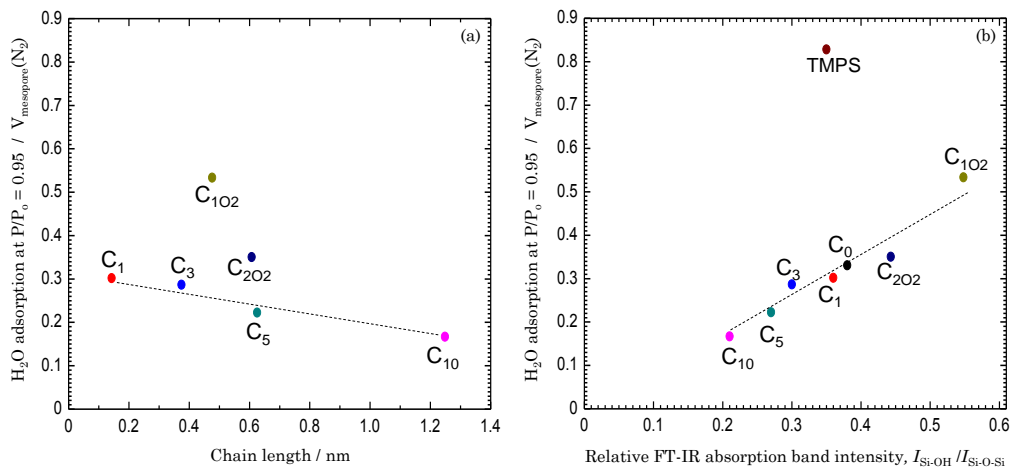

Fig. 4-10. Relative amount of water adsorbed within the mesopores at $P/P_o = 0.95$ as a function of (a) chain length of alkoxy group (OR), and (b) hydroxyl group density.

As shown in Fig. 4-11, except for C_{10}, the mean mesopore size in the PHPS-derived samples was larger than 10 nm. H_2O adsorption by these samples is thus thought to have been largely controlled by the density of OH groups. In contrast, the mean mesopore size for C_{10} was

3.3 nm, a value close to that of TMPS (3.7 nm), and C_{10} exhibited much lower H_2O adsorption.

Fig. 4-12 presents a schematic summarizing the proposed factors determining the H_2O adsorption properties of the PHPS-derived amorphous silica-based hybrid samples investigated in this study. Following the completion of the first hydration layer, subsequent water adsorption leads to multilayer adsorption as capillary condensation begins to occur with increasing P/P_o. With regard to the initial hydration layer formation, $R'OC_2H_4$ ($R'= CH_3$ and/or C_2H_5) groups were, to some extent, effective at suppressing H_2O adsorption by interaction with Si-OH groups. However, for multilayer adsorption at higher humidity, these groups were no longer effective due to their polarity. As shown in Fig. 4-11, capillary condensation behaved differently, depending on the mesopore size. For mesopores larger than 10 nm, capillary condensation was basically governed by the density of Si-OH groups while, in the case of mesopores smaller than 4 nm, the data suggest that the relatively long, hydrophobic n-$C_{10}H_{21}$ groups suppressed capillary condensation.
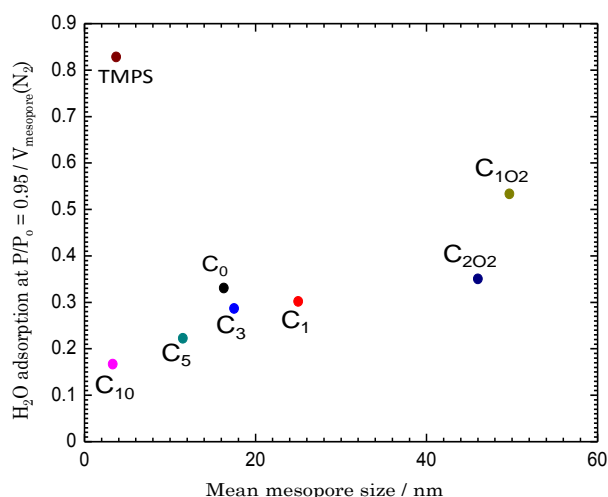

Fig. 4-11. Relative amount of water adsorbed within the mesopores at $P/P_o = 0.95$ as a function of mean mesopore size.

In addition to the minimum OH group density established in Fig. 4-9(b), the hydrophobic nature of the mesopores in the n-$C_{10}H_{21}O$ hybrid suggest the potential of the polymer route employed in this study to synthesize hydrostable amorphous silica-based materials for energy applications, such as in H_2 production from photocatalytic water splitting processes at room temperature.

It is also interesting to note that the polymer derived ceramics (PDCs) route in this study show some potential to synthesize mesoporous materials with high surface area. This can be

achieved by manipulating the chain length and types of alcohols used for the modification of PHPS, as listed in Table 4-1. However, it was not achieved for our samples that the controlled pore dimensions and large pore volume which are typical for mesoporous materials. Recently, Bernard *et al*. [30] reported that novel non-oxide mesoporous materials can be synthesized by combination of PDCs route and nanocasting process [31] using ordered mesoporous carbon as a hard template, and the ordered mesoporosity with high specific surface area was successfully achieved for binary B-N and quaternary Si-B-C-N ceramic systems. Polysilazanes are essentially soluble and fusible polymer precursors, thus expected to be applied for synthesizing novel mesoporous metal oxides through organic–inorganic assembly processes by using surfactants or block copolymers as soft templates [32]. Moreover, for the synthesis of mesoporous materials with enhanced surface area and simultaneous improvement in pore dimensions and pore volume, it is also attractive to combine this PDCs route with novel LbL (layer by layer) method for thin-film preparation of mesoporous materials which recently reviewed by Ariga *et al*. [33]. These synthetic approaches may also find useful applications in various fields where moisture resistance and/or hydrophobic surface nature are required.
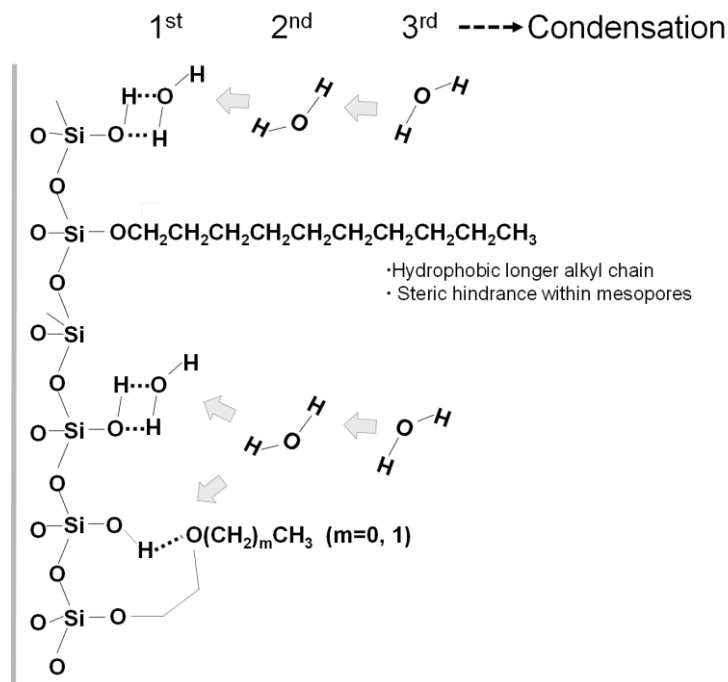

Fig. 4-12. Schematic showing factors determining the H_2O adsorption properties of the PHPS-derived amorphous silica-based hybrids investigated in this study.

4.4. Conclusion

In this study, PHPS was chemically modified with various alcohols (ROH, R = CH_3, n-C_3H_7, n-C_5H_{11}, n-$C_{10}H_{21}$, $CH_3OC_2H_4$, $C_2H_5OC_2H_4$) at a PHPS (Si basis)/ROH molar ratio of 3:1. The alkoxy group-functionalized PHPS was successfully converted to amorphous silica-based inorganic-organic hybrid materials by a room temperature oxidation technique, and the hydrophilic/hydrophobic properties of these materials were studied by comparison to a commercial mesoporous silica powder with a mean mesopore size of 3.7 nm. The results may be summarized as follows.

(1) Nitrogen sorption analysis revealed that the PHPS-derived silica-based hybrid samples exhibited a small quantity of micropores less than 0.9 nm in size and, except for the methoxyethyl- and ethoxyethyl-group functionalized samples, there was a tendency for the specific surface area to increase with increasing number of carbon atoms in the alkoxy groups. In addition, the mean mesopore size decreased with increasing number of carbon atoms. As a result, the specific surface area and mean mesopore size for the n-$C_{10}H_{21}O$ group-functionalized hybrid were 456.5 m^2/g and 3.3 nm, respectively.

(2) H_2O sorption analysis showed that, at lower humidity of $P/P_o \leq 0.6$, H_2O adsorption was governed by the density of Si-OH groups. However, at higher humidity of $P/P_o > 0.6$, H_2O adsorption for the samples was apparently lower than that for the commercial mesoporous silica.

(3) The data suggest that the addition of $R'OC_2H_4$ (R' = CH_3 and/or C_2H_5) groups is effective at suppressing H_2O adsorption during the initial hydration layer formation. However, these groups did not affect multilayer adsorption at higher humidity, due to their polarity.

(4) The amorphous silica-based hybrid synthesized from PHPS modified with n-$C_{10}H_{21}OH$ was found to exhibit stable performance without significant capillary condensation even at higher humidity above $P/P_o = 0.6$. As a result, the number of water molecules adsorbed per square nanometre of the sample surface area at $P/P_o = 0.95$ was as low as 4 mol nm^{-2}.

(5) The lower density of hydrophilic silanol groups (0.21), smaller mesopore size (3.3 nm) and longer hydrophobic chain of the n-$C_{10}H_{21}O$ group (1.248 nm) all likely contributed to the improved hydrophobicity of this sample. These results indicate that the polymer precursor route investigated in this study has the potential to allow the development of hydrostable amorphous silica-based membranes for hydrogen gas separation with applications to photocatalytic water splitting processes.

References

[1] K. Maeda, K.Domen, J. Phys. Chem., C 111 (2007) 7851-7861.

[2] Y. Iwamoto, J. Ceram. Soc. Japan, 115 (2007) 947-954.

[3] K. Tanaka, Y. Sakata, Membrane, 36 (2011) 113-121.

[4] T. Tsuru, R. Igi, M. Kanezashi, T. Yoshioka, S. Fujisaki, Y. Iwamoto, AIChE J. 57 (2011) 618-629.

[5] V. Rao, M. M. Kulkarni, D. P. Amalnerkar, T. Seth, Appl. Surf. Sci., 167 (2003) 262-270.

[6] H. El Rassy, A. C. Pierre, J. Non-Cryst. Solids, 351 (2005) 1603-1610.

[7] J. Mecinovic, P.W. Snyder, K.A. Mirica, S. Bai, E.T. Mack, R.L. Kwant, D.T. Moustakas, A. Heroux, G. M. Whitesides, J Am. Chem. Soc., 133 (2011) 14017-26.

[8] F. Schwertfeger, N. Hüsing, U. Schubert, J. Sol-Gel Sci. Technol., 2 (1994) 103-108.

[9] N. Gokulakrishnan, T. Karbowiak, J.P Bellat, L. Vonna, M. Saada, J.L Paillaud, M. Soulard, J. Patarin, J. Parmentier, Colloids Surf., A 421 (2013) 34-43.

[10] Y. Iwamoto, K. Sato, T. Kato, T. Inada, Y. Kubo, J. Eur. Ceram. Soc., 25 (2005) 257-264.

[11] T. Kubo, H. Kozuka, J. Ceram. Soc. Japan, 114 (2006) 517-523.

[12] M. Monti, B.D. Bianco, R. Bertoncello, S. Voltolina, J. Cult. Herit., 9 (2008) 143-145.

[13] Y. Iwamoto, K. Kikuta, S. Hirano, J. Mater. Res., 13 (1998) 353-361.

[14] M.N.M. Sokri, Y. Daiko, S. Honda, Y. Iwamoto, J. Ceram. Soc. Jpn., 123, (2015) 292-297.

[15] M.N.M. Sokri, T. Onishi, Z. Mouline, Y. Daiko, S. Honda, Y. Iwamoto, J. Ceram. Soc. Jpn., 123, (2015) 732-738.

[16] D.F. Shiver, M.A. Drezdzon, "The manipulation of air sensitive compounds", J. Wiley & Sons, New York, (1986).

[17] A. Saito, H.C. Foley, AIChE J., 37 (1991) 429-436.

[18] P. Barrett, L.G. Joyner, P.P. Halenda, J. Am. Chem. Soc., 73 (1951) 373-380.

[19] D. Seyferth, G. Wiseman, C. Prud'homme, J. Am. Ceram. Soc., 66 (1983) C-13-C-14.

[20] D.Seyferth, C.Strohmann, N.R. Dando, A. Perrotta, J. Chem. Mater., 7 (1995) 2058-2066.

[21] R.M. Silverstein, G.C. Bassler, T. C. Morrill, "Spectrometric Identification of Organic Compounds", J. Wiley & Sons, New York, (1991).

[22] Y. Iwamoto, K. Kikuta, S. Hirano, J. Mater. Res., 14 (1999) 1886-1895.

[23] K.S.W. Sing, D.H. Everett, R.A.W. Haul, L. Moscou, R.A. Pierotti, J. Rouquerol, T. Siemieniewska, Pure Appl. Chem., 57 (1985) 603-619.

[24] S. Lowell, J.E. Shields, M.A. Thomas, M. Thommes, "Characterization of Porous Solid and Powders", Springer, Netherlands, (2004).

[25] T. Ishikawa, M. Matsuda, A. Yasukawa, K. Kandori, S. Inagaki, T. Fukushima, S. Kondo, J. Chem. Soc., Faraday Trans., 92 (1996) 1985-1989.

[26] A. Burneau, J. Lepage, G. Maurice, J. Non-Cryst. Solids, 217 (1997) 1-10.

[27] A.A. Chuiko, React. Kinet. Catal. Lett., 50 (1993) 1-13.

[28] E.A. Leed, C.G. Pantano, J. Non-Cryst. Solids, 325 (2003) 48-60.

[29] P. Lodewyckx, D. Van Rompaey, L. Verhoeven, E.F. Vansant, Carbon, 39, (2001) 309-310.

[30] S. Bernard, P. Miele, New J. Chem., 38, (2014) 1923-1931.

[31] D. Gu, F. Schüth, Chem. Soc. Rev., 43, (2014) 313-344.

[32] K. Ariga, A. Vinu, Y. Yamauchi, Q. Ji, J. P. Hill, Bull. Chem. Soc. Jpn., 85, (2012) 1-32.

[33] K. Ariga, Y. Yamauchi, G. Rydzek, Q. Ji, Y. Yonamine, K.C. Wu, J.P. Hill, Chem. Lett., 43, (2014) 36-68.

Chapter 5. Summary

The objective of this thesis was to develop novel meso- and microporous structure control technologies for amorphous silica-based materials to develop gas separation membranes operated at lower temperatures below 100 ℃. In this study, perhydropolysilazanes (PHPSs) having alkoxy groups as a sacrificial template for meso- and micropore formation were designed and synthesized. The effects of alkoxy chain length and *in-situ* gases formation during the thermal conversion of polymer to amorphous silica were investigated. Moreover, the hydrophobicity of amorphous silica-based inorganic-organic hybrids was studied for the room temperature application under the co-existence of water vapour such as novel solar hydrogen production system.

In Chapter 1, recent research articles related to ceramics gas separation membranes, ceramic processing techniques and porous structure controlling have been briefly reviewed, and the above mentioned objectives of present study were described.

In Chapter 2, commercially available PHPS was chemically modified with various alcohols with different carbon chain length to afford alkoxy-group functionalized PHPS. The alkoxy-group functionalized PHPS was then converted into amorphous silica powders by oxidative crosslinking at 270°C and subsequent pyrolysis at 600°C. Based on FT-IR and ^{1}H-NMR spectroscopic analyses, the alcohol mainly reacted with H_2SiN_2 groups of PHPS to form $RO-SiHN_2$ groups. The TG analysis indicated that the thermal decomposition of the alkoxy groups introduced to PHPS was found to be essential for the microporous structure development The pore size distribution of the 600°C-pyrolyzed samples showed that the microporosity increased with the number of carbon atom of alcohol used as a chemical modifier for PHPS, and the introduction of $n-C_{10}H_{21}O$ groups resulted in a significant increase in the micropore volume. Further enhancement in the micropore volume could be achieved when increasing the amount of $n-C_{10}H_{21}OH$ used in the chemical modification.

In Chapter 3, based on the results described in Chapter 2, $n-C_5H_{11}O$ and $n-C_{10}H_{21}O$ groups functionalized PHPSs were selected and converted to amorphous silica-based inorganic-organic hybrids under room temperature oxidation. To study the microporosity formation in more detail, the thermal conversion of the resulting hybrids to amorphous silica was *in-situ* monitored by using a TG-MS analyser. It was concluded that the in-situ formed small gas species such as CO_2 gas molecules and C3 and C4 hydrocarbon unit could mainly contribute to develop the microporous structure.

In Chapter 4, by using room temperature oxidation technique described in Chapter 3, alkoxy group-functionalized PHPS was converted to amorphous silica-based inorganic-organic hybrid powders, and the hydrophilic/hydrophobic properties of these materials were studied and

evaluated by comparing with a commercial mesoporous silica powder with a mean mesopore size of 3.7 nm. Based on nitrogen sorption analysis, the PHPS-derived amorphous silica-based hybrid samples exhibited a wide pore size distribution having mean mesopore sizes ranging from 3.3 nm up 49.7 nm, with a small quantity of micropores smaller than 0.9 nm in size. In addition, the mean mesopore size decreased with increasing number of carbon atoms, i.e., alkoxy chain length. H_2O sorption analysis revealed that at lower humidity of $P/P_o < 0.6$, H_2O adsorption was found to be governed by the density of Si-OH groups calculated from FT-IR absorption band intensity ratio of $I_{Si-OH}/I_{Si-O-Si}$. The amorphous silica-based hybrid derived from PHPS modified with n-$C_{10}H_{21}OH$ was found to exhibit stable performance without significant capillary condensation even at higher humidity of $P/P_o > 0.6$. As a result, the number of water molecules adsorbed per square nanometre of the sample surface area at $P/P_o = 0.95$ was as low as 4 mol nm^{-2}, which was lowest among the samples. The improved hydrophobicity of this sample was considered to be achieved by the plural effects derived from the lower density of silanol groups (0.21), the smaller mean mesopore size (3.3 nm) and the longer hydrophobic alkoxy chain length.

List of publications and presentation in conference

1. Original papers

(1) "Synthesis of microporous amorphous silica from perhydropolysilazane chemically modified with alcohol derivatives" (Chapter 2)

Mohd Nazri Mohd Sokri, Yusuke Daiko, Sawao Honda and Yuji Iwamoto

Journal of the Ceramic Society of Japan, 123, 292-297 (2015). Impact Factor: 0.846.

(2) "Polymer-derived amorphous silica-based inorganic-organic hybrids having alkoxy groups: intermediates for synthesizing microporous amorphous silica materials" (Chapter 3)

Mohd Nazri Mohd Sokri, Takahiro Onishi, Zineb Mouline, Yusuke Daiko, Sawao Honda and Yuji Iwamoto

Journal of the Ceramic Society of Japan, 123, 732-738 (2015). Impact Factor: 0.846

(3) "Hydrophobicity of amorphous silica-based inorganic-organic hybrid materials derived from perhydropolysilazane chemically modified with alcohols" (Chapter 4)

Mohd Nazri Mohd Sokri, Takahiro Onishi, Yusuke Daiko, Sawao Honda and Yuji Iwamoto

Microporous and Mesoporous Materials, 215, 183-190 (2015). Impact Factor: 3.209

2. Presentation at international conferences

(1) Polymer-derived Microporous Amorphous Silica

Mohd Nazri Mohd Sokri, Sawao Honda and Yuji Iwamoto

The 3rd International Symposium on Ceramics Nanotune Technology (ISCeNT-3), Nagoya, Japan (March, 2-4, 2014), Oral presentation.

Acknowledgements

March 2016

Mohd Nazri bin Mohd Sokri